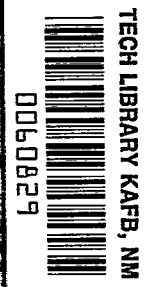


NASA CONTRACTOR
REPORT



NASA CR-1544



NASA CR-1544

LOAN COPY: RETURN TO
AFWL (WL0L)
KIRTLAND AFB, N MEX

WAKE ANALYSIS FOR SUPERSONIC DECCELERATOR APPLICATIONS

Volume II - Application of Gas-Hydraulic Analogy
to Shallow-Water Tow Channel Results

by *Richard A. Lau*

Prepared by
GOODYEAR AEROSPACE CORPORATION
Akron, Ohio
for Langley Research Center



NASA CR-1544

TECH LIBRARY KAFB, NM



0060829

WAKE ANALYSIS FOR
SUPERSONIC DECELERATOR APPLICATIONS
Volume II - Application of Gas-Hydraulic Analogy to
Shallow-Water Tow Channel Results

By Richard A. Lau

Distribution of this report is provided in the interest of information exchange. Responsibility for the contents resides in the author or organization that prepared it.

Prepared under Contract No. NAS 1-8010 by
GOODYEAR AEROSPACE CORPORATION
Akron, Ohio

for Langley Research Center

NATIONAL AERONAUTICS AND SPACE ADMINISTRATION

For sale by the Clearinghouse for Federal Scientific and Technical Information
Springfield, Virginia 22151 - CFSTI price \$3.00

PREFACE

The work described in this document was performed by Goodyear Aerospace Corporation, Akron, Ohio under NASA Contract NAS1-8010, Supersonic Decelerator Wake Studies. Results of these studies are presented in two volumes:

Volume I - Theoretical Analysis and Correlation of
Wind Tunnel and Shallow-Water Tow
Channel Results (NASA CR-1543)

Volume II - Application of Gas Hydraulic Analogy to
Shallow-Water Tow-Channel Results

Contractor's number for this report is GER-14330.

*Basic to
Speed of Sound
Wake*

-

7

1

-

-

CONTENTS

		<u>Page</u>
PREFACE		iii
SUMMARY		xiii
<u>Section</u>	<u>Title</u>	
I	INTRODUCTION	1
II	APPLICATION OF THE WATER-GAS ANALOGY.	3
	1. Gas-Hydraulic Analogy	3
	a. Previous Studies	3
	b. Results	3
	2. Experimental Considerations	5
	a. Water Depth	5
	b. Model Size	5
	c. Tow Channel Versus Water Flow Channel	5
	3. Analogy Development and Modifications	6
III	TEST FACILITY	11
	1. Tow Channel and Instrumentation	11
	2. Photographic Equipment	11
	a. Sequence Still Camera	11
	b. Stereophotogrammetric Camera/Projector Equipment	12
IV	SUMMARY OF TEST RUNS AND CONDITIONS	17
	1. Description of Test Models	17
	2. Summary of Tests	17
	3. Experimental Procedure	17
V	RESULTS	23
	1. Sequence Still Data	23
	a. Data Treads	23
	b. Angle-of-Attack Effects on the Hydraulic Jump	32
	c. Comparison of Hydraulic Jump and Theoretical Gas Shock Results	32
	2. Stereo Data	32
VI	CONCLUSIONS	39

CONTENTS

<u>Appendix</u>	<u>Title</u>	<u>Page</u>
A	PRINCIPLES OF THE GAS-HYDRAULIC ANALOGY .	41
B	REPRESENTATIVE TOW CHANNEL STILL PHOTO- GRAPHS	49
	LIST OF SYMBOLS	61
	LIST OF REFERENCES	63

ILLUSTRATIONS

Figure	Title	Page
1	Theoretical Correlation Between Water and Air Characteristics Across an Oblique Bow Wave ($\delta = 9$ Deg)	6
2	Static Depth and Density Ratios Across Oblique Wave as Function of Upstream Mach (Froude) Number . . .	9
3	Sequence Still Photographic Technique	13
4	Stereophotogrammetric Technique	14
5	Effects of Free-Stream Froude Number on Circular Cylinder Data	24
6	Effects of Deflection Angle and Model Size on Wedge Data	25
7	Effects of Shoulder Radius on 80- and 120-Deg Wedge Data	26
8	Effects of Free-Stream Froude Number on Ogive-Block Configuration	27
9	Effects of Free-Stream Froude Number on Half Cylinder-Block Configuration	28
10	Effects of Flare Length on Half Cylinder-Block-Flare Configuration	29
11	Effects of Flare Angle on Half Cylinder-Block-Flare Configurations	30
12	Effects of Free-Stream Froude Number and Nose Geometry on Block Configuration with Different Nose Shapes	31
13	Comparison of Attached Hydraulic Jump Geometry with Oblique Shock Theory at Mach (Froude) Number of 2	33
14	Comparison of Attached Hydraulic Jump Geometry with Oblique Shock Theory at Mach (Froude) Number of 2.5	34
15	Stereo Contour Map at $Fr_{\infty} = 2.2$ (Wedge Block Forebody and Reversed Half Cylinder Trailing Body) . . .	35

<u>Figure</u>	<u>Title</u>	<u>Page</u>
16	Stereo Contour Map at $Fr_{\infty} = 2.2$ (120-Deg Wedge Forebody and Reversed Half Cylinder Trailing Body)	36
17	Stereo Contour Map at $Fr_{\infty} = 2.2$ (Blunted Wedge Block-Flare Forebody and Reversed Half Cylinder Trailing Body)	37
18	Flow of Incompressible Fluid	41
19	Surface Wave Propagation Velocity as a Function of Wavelength	48
20	Wedge-Block ($Fr_{\infty} = 2.0$)	50
21	Wedge-Block ($Fr_{\infty} = 2.5$)	50
22	80-Deg Wedge ($Fr_{\infty} = 2.0$)	51
23	80-Deg Wedge ($Fr_{\infty} = 2.5$)	51
24	Circular Cylinder ($Fr_{\infty} = 2.0$)	52
25	Circular Cylinder ($Fr_{\infty} = 2.5$)	52
26	Half Cylinder-Block-Flare ($Fr_{\infty} = 2.0$)	53
27	Half Cylinder-Block-Flare ($Fr_{\infty} = 2.5$)	53
28	Blunted Wedge-Block-Flare ($Fr_{\infty} = 2.0$)	54
29	Blunted Wedge-Block Flare ($Fr_{\infty} = 2.5$)	54
30	120-Deg Wedge with Trailing 10-Deg Wedge ($Fr_{\infty} = 2.0, x/D = 2.0$)	55
31	120-Deg Wedge with Trailing 10-Deg Wedge ($Fr_{\infty} = 2.5, x/D = 2.0$)	55
32	Wedge-Block with Trailing Reversed Half Cylinder ($Fr_{\infty} = 2.0, x/D = 9$)	56
33	Wedge-Block with Trailing Reversed Half Cylinder ($Fr_{\infty} = 2.5, x/D = 9$)	56
34	Wedge-Block at $\alpha = 5$ Deg with Trailing Reversed Half Cylinder ($Fr_{\infty} = 2.0, x/D = 9$)	57
35	Wedge-Block at $\alpha = 5$ Deg with Trailing Reversed Half Cylinder ($Fr_{\infty} = 2.5, x/D = 9$)	57

<u>Figure</u>	<u>Title</u>	<u>Page</u>
36	120-Deg Wedge with Trailing Reversed Half Cylinder ($Fr_{\infty} = 2.0, x/D = 8.5$)	58
37	120-Deg Wedge with Trailing Reversed Half Cylinder ($Fr_{\infty} = 2.5, x/D = 8.5$)	58
38	120-Deg Wedge at $\alpha = 5$ Deg with Trailing Reversed Half Cylinder ($Fr_{\infty} = 2.0, x/D = 8.5$)	59
39	120-Deg Wedge at $\alpha = 5$ Deg with Trailing Reversed Half Cylinder ($Fr_{\infty} = 2.5, x/D = 8.5$)	59

TABLES

<u>Table</u>	<u>Title</u>	<u>Page</u>
I	Analogous Relations, Gas-Hydraulic Analogy	4
II	Analogous Terms and Conditions, Gas-Hydraulic Analogy	4
III	Test Configurations	19
IV	Tow Channel Test Summary (Sequence Still Photographic Techniques)	21
V	Tow Channel Test Summary (Stereo Photographic Techniques)	22

SUMMARY

The theoretical and experimental use of the shallow water tow channel was investigated for predicting characteristics of a two-dimensional compressible gas. This investigation included a study of the gas-hydraulic analogy and methods for extending its application to water flows containing hydraulic jumps. Tow channel tests also were conducted on a wide variety of two-dimensional configurations.

The results of this investigation tend to support the use of the tow channel as a means of qualitatively studying two-dimensional compressible flows and indicate that certain quantitative aspects of these flows are accurately predicted by tow channel data.

WAKE ANALYSIS FOR SUPERSONIC DECELERATOR APPLICATIONS

Volume II - Application of Gas-Hydraulic
Analogy to Shallow-Water Tow-Channel Results

By Richard A. Lau
Goodyear Aerospace Corporation

SECTION I - INTRODUCTION

A portion of the supersonic wake analysis program investigated the shallow-water tow channel and the analogous relationship between (1) flows of incompressible water having a free surface, and (2) a two-dimensional compressible gas. The analogous nature of these two flows has been the subject of many previous studies (e.g., References 1 through 5). In general, the studies have shown that a water flow is useful in studying compressible flows, in particular the qualitative aspects of such flows and in the visualization of their flow patterns.

This investigation was directed toward a study of compressible wakes with the use of the tow channel and was carried out in conjunction with the development and analysis of a theoretical wake solution (see Volume I). Knowledge of compressible wakes is important for advancing decelerator technology because the decelerator typically must operate in the nonuniform wake stream.

The tow channel is analyzed as a potential wake research tool in Volume I. Volume II contains (1) a discussion and development of the mathematical water-gas relationships, (2) a description of the facility and equipment used and the procedures employed, and (3) a presentation and analysis of data obtained.

All tow-channel tests were conducted at Wright-Patterson Air Force Base, Dayton, Ohio. Technical assistance and advice were given by Mr. C. A. Babish III of the Flight Dynamics Laboratory (FDFR).

SECTION II - APPLICATION OF THE WATER-GAS ANALOGY

1. Gas-Hydraulic Analogy

a. Previous Studies

The mathematical relationships existing between a flow of water having a free surface and a two-dimensional compressible gas are set forth in the gas-hydraulic analogy. Probably the most notable work on this analogy is that of Preiswerk^{1, a} who, in 1938, provided conclusive proof that the methods of gas-dynamics can be applied to a water flow. Since that time, several other studies (e.g., References 2 through 5) of the gas-hydraulic analogy and its applications have been made.

A derivation of the basic relationships, based primarily on the mathematical developments presented in References 1 through 5, is provided in Appendix A.

b. Results

The basic assumptions employed in the development of the gas-hydraulic analogy are:

1. Frictionless and adiabatic flow
2. Irrotational flow
3. Negligible vertical accelerations compared with gravity

The major limitations imposed by its derivation are:

1. Strictly analogous only to $\gamma = 2$ gas
2. Representative of two-dimensional flow
3. Restricted to shallow water (depths, $d \ll$ wavelength, λ)
4. Change in internal energy across a shock wave not equivalent between water and gas

Tables I and II summarize the mathematically derived relationships and the analogous terms and conditions between a flow of water and a two-dimensional gas flow. From the assumptions and limitations data, it is apparent that the analogy is completely valid only when the analogous gas is two-dimensional, irrotational, and isentropic and has a specific heat ratio of 2 (see Appendix A). These characteristics are not all fulfilled by any real gas and are used to describe the hypothetical "hydraulic gas."

^aSuperior numbers in the text refer to items in the List of References.

TABLE I - ANALOGOUS RELATIONS, GAS-HYDRAULIC ANALOGY

Compressible fluid	Water
Two-dimensional gas flow	Flow of liquid with free surface in gravity field
$\gamma = 2$ gas	Incompressible fluid (water)
Velocity, $\frac{V}{V_{\max}}$	Velocity, $\frac{V}{V_{\max}}$
Pressure, $\frac{P}{P_0}$	(Depth) ² , $\left(\frac{d}{d_0}\right)^2$
Density, $\frac{\rho}{\rho_0}$	Depth, $\frac{d}{d_0}$
Temperature, $\frac{T}{T_0}$	Depth, $\frac{d}{d_0}$
Sonic velocity, $a = \sqrt{\gamma g R T}$	Surface wave propagation velocity, $c = \sqrt{gd}$
Mach number, $M = \frac{V}{a}$	Froude number, $Fr = \frac{V}{\sqrt{gd}}$

TABLE II - ANALOGOUS TERMS AND CONDITIONS,
GAS-HYDRAULIC ANALOGY

Compressible fluid	Water
Subsonic flow	Streaming flow
Supersonic flow	Shooting flow
Normal shock wave	Right hydraulic jump
Oblique shock wave	Slant hydraulic jump
Flow expansion	Level drop
Flow compression	Level rise
Expansion wave	Depression wave
Wave pulsation	Hydraulic jump oscillation

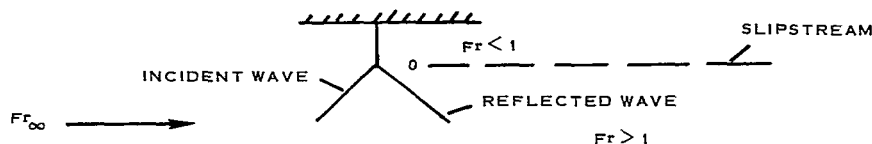
2. EXPERIMENTAL CONSIDERATIONS

a. Water Depth

In this test program, a nominal water depth of 0.19 in. was used. This value was selected based upon the results of Reference 3 (see Appendix A, Item 2). In Item 2, it is shown that, for water depths of about 0.2 in., the surface wave propagation velocity, c , is equal to \sqrt{gd} and, thus, is analogous to the sonic velocity, a , in a compressible gas. For other depths, c is a function of the wavelength, λ , for which there is no counterpart in the analogy. Gupta⁶ has shown, theoretically, that the optimum water depth is 0.19 in.

b. Model Size

Because wavelength, λ , is a direct function of the model size,⁵ it generally is desirable to use large models and, thus, reduce the effect of capillary ripples ($\lambda \leq 1$ in.). As a practical matter, the model size generally is limited to the size of the available tow channel (or flow channel) and to the geometry of the model being tested. In this program, for example it was found that 4-in. wide blunt models represented a practical limit in a 4-ft-wide tow channel. When larger models were tested, wall effects were typically experienced, particularly at lower free-stream Froude number, Fr_{∞} , values. In these cases, the bow hydraulic jump was reflected from the wall in such a manner that the incident and reflected wave formed a triple intersection point at 0 (see sketch below)



The intersection point, 0, then would propagate upstream until the bow wave was completely normal to the direction of the free-stream flow.

c. Tow Channel Versus Water Flow Channel

All tests were conducted in a tow channel - that is, a channel in which the model is moved through still water. The major advantage of a tow channel over a flow channel (one in which a flow of water is passed around a still model) is that no velocity gradients are produced from the channel floor or walls. This is of particular importance since a shallow depth (0.2 in.) should be used to obtain the proper analogy. A problem with tow channels is the difficulty generally experienced in obtaining accurate depth measurement in the water flow. In this program, these measurements were obtained using a camera system that provided a three-dimensional stereomodel of the test configuration and surrounding flow. This camera system is discussed in greater detail later.

3. ANALOGY DEVELOPMENT AND MODIFICATIONS

The gas-hydraulic analogy, as summarized in Item 1, above, is strictly valid only when the isentropic flow of a hypothetical, compressible, two-dimensional gas ($\gamma = 2$) is considered. When simulating supersonic air-flow through a shock wave, the analogy is imperfect for two basic reasons: (1) $\gamma = 1.4$ for air while the analogy requires $\gamma = 2$ and (2) the analogy requires that the change in entropy $\Delta s = 0$ across the shock, a condition not fulfilled by any real gas.

Under certain simulation conditions, however, these two imperfections actually tend to compensate for one another across a hydraulic jump. Harleman,⁷ for example, used a slender cone ($\delta = 9$ deg) in a water flow to show that the properties downstream of an attached two-dimensional air shock wave from a corresponding body could be obtained with good accuracy using the "first modification of the direct analogy." Basically, this method relies upon obtaining the static density ratio across a shock from the static depth value across a hydraulic jump and then computing other gas properties from conventional gas dynamic relationships. The depth ratio was used to predict density ratios because the best correlation was found to exist between these two parameters (see Figure 1). At Mach 3, the relative error using the depth ratio to predict the density ratio is about 2 percent; at Mach 9, the error is about 8 percent.

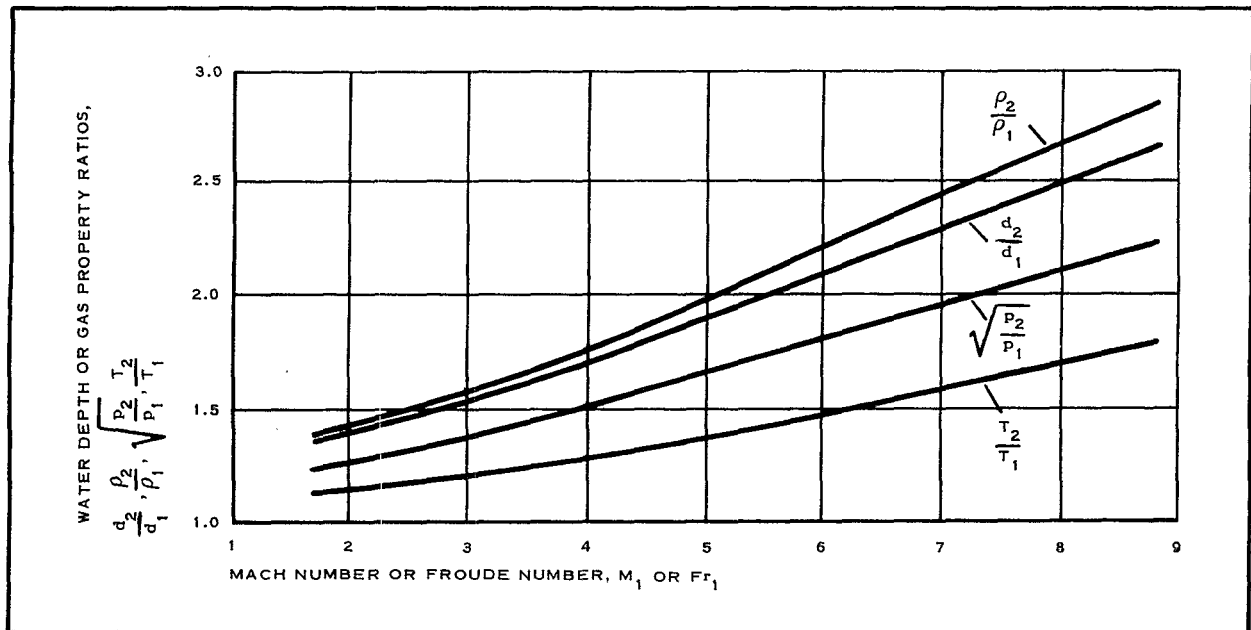


Figure 1 - Theoretical Correlation Between Water and Air Characteristics Across an Oblique Bow Wave ($\delta = 9$ Deg)

It is shown in Volume I, however, that the first modification approach is approximately valid only when small deflection angles are considered. This primarily results from the small deflection angles producing attached bow waves that are nearly independent of γ .

For larger deflection angles with curved and, possibly, detached bow waves, the first modification method is no longer conceptually applicable. First, the wave shape can no longer be considered as independent of γ ; therefore, the wave shape in water theoretically is no longer similar to that in two-dimensional compressible air. Second, the airflow behind a curved shock is highly rotational due to the entropy gradients produced, and water results are not applicable to this type of flow. Because it may be possible experimentally to achieve situations where reasonable agreement is obtained between water hydraulic jump and two-dimensional air shock waves, the quantitative application of water flow to compressible gas flow must be considered for these cases. Babish⁸ has presented the necessary relationships to describe theoretically the physical change in water passing through a hydraulic jump.

Equations for the normal hydraulic jump are:

$$\frac{d_2}{d_1} = \left(2Fr_1^2 + \frac{1}{4} \right)^{\frac{1}{2}} - \frac{1}{2}, \quad (1)$$

$$\frac{d_{2o}}{d_1} = \left(\frac{d_2}{d_1} \right) + \frac{1}{4} \left[1 + \left(\frac{d_2}{d_1} \right)^{-1} \right], \text{ and} \quad (2)$$

$$Fr_2^2 = \frac{1}{2} \left[1 + \frac{1}{\left(\frac{d_2}{d_1} \right)} \right]^2 - \frac{1}{8}. \quad (3)$$

Equations for a slant hydraulic jump are given below.

$$\frac{d_2}{d_1} = \left(2Fr_1^2 \sin^2 \theta + \frac{1}{4} \right)^{\frac{1}{2}} - \frac{1}{2}. \quad (4)$$

$$\frac{d_{2o}}{d_1} = \frac{\left[4 \left(\frac{d_2}{d_1} \right) + 1 + \frac{1}{\left(\frac{d_2}{d_1} \right)} \right] \left\{ 1 + \frac{1}{4 \sin^2 \theta} \left[\left(\frac{d_2}{d_1} \right)^2 + \frac{d_2}{d_1} \right] \right\}}{\left(\frac{d_2}{d_1} \right)^2 + \left(\frac{d_2}{d_1} \right) + 4}. \quad (5)$$

$$Fr_2^2 \sin^2(\theta - \delta) = \frac{1}{2} \left[\frac{1}{2} + \frac{1}{\left(\frac{d_2}{d_1}\right)} \right]^2 - \frac{1}{8}, \quad (6)$$

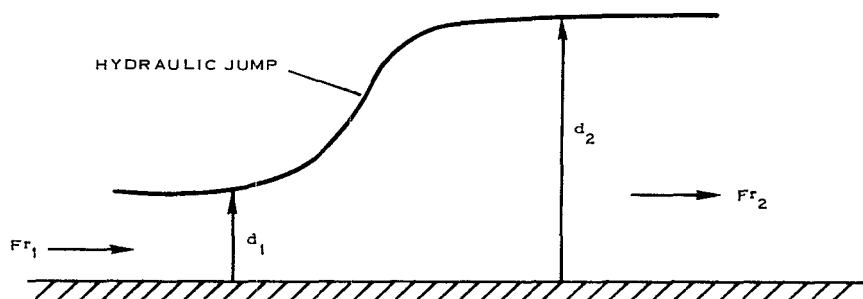
where

Fr = Froude number;

d = water height;

subscripts 0, 1, and 2 = stagnation, prehydraulic jump, and post hydraulic jump conditions respectively (see sketch); and

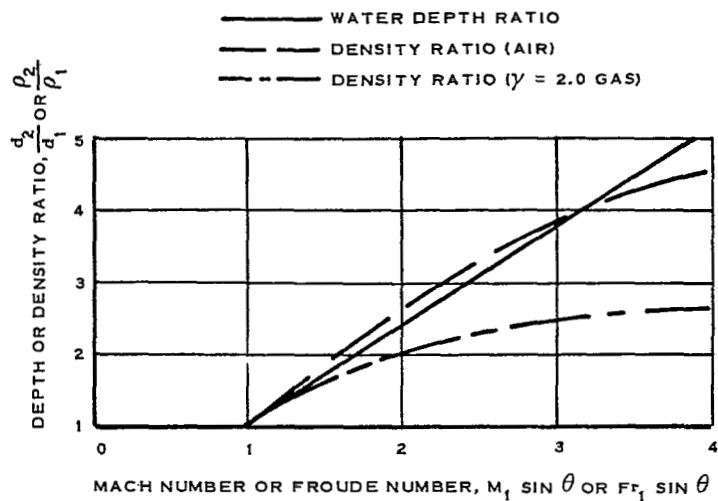
$$\delta = \tan^{-1} \left\{ \frac{\tan \theta \left[\left(1 + 8Fr_1^2 \sin^2 \theta \right)^{\frac{1}{2}} - 3 \right]}{\left(2 \tan^2 \theta - 1 \right) + \left(1 + 8Fr_1^2 \sin^2 \theta \right)^{\frac{1}{2}}} \right\}. \quad (7)$$



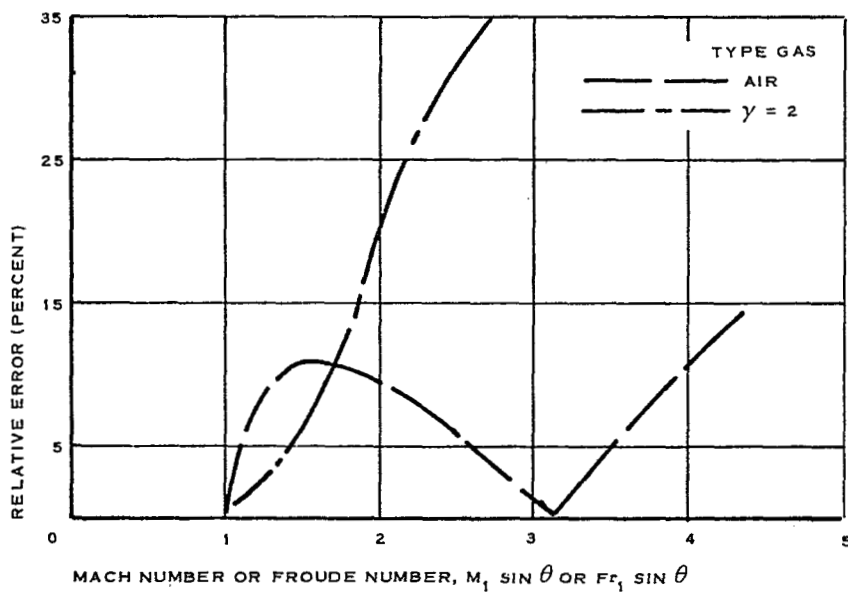
When the results of Equation (4), for example, are compared with the density ratio across a shock as predicted by the gas-dynamic relationship,

$$\frac{\rho_2}{\rho_1} = \frac{(\gamma + 1) M_1^2 \sin^2 \theta}{(\gamma - 1) M_1^2 \sin^2 \theta + 2}, \quad (8)$$

reasonable agreement is found to exist within a range of Mach (Froude) $\sin \theta$ values between 1 and 4. This is shown in Figure 2, where, within this range, an error of about 10 percent or less is incurred for air. For $\gamma = 2$ gas, the error becomes prohibitively large at relatively low values of $M_1 \sin \theta$. It should be noted that the results of Figure 2 actually constitute a part of the justification of the first modification approach.

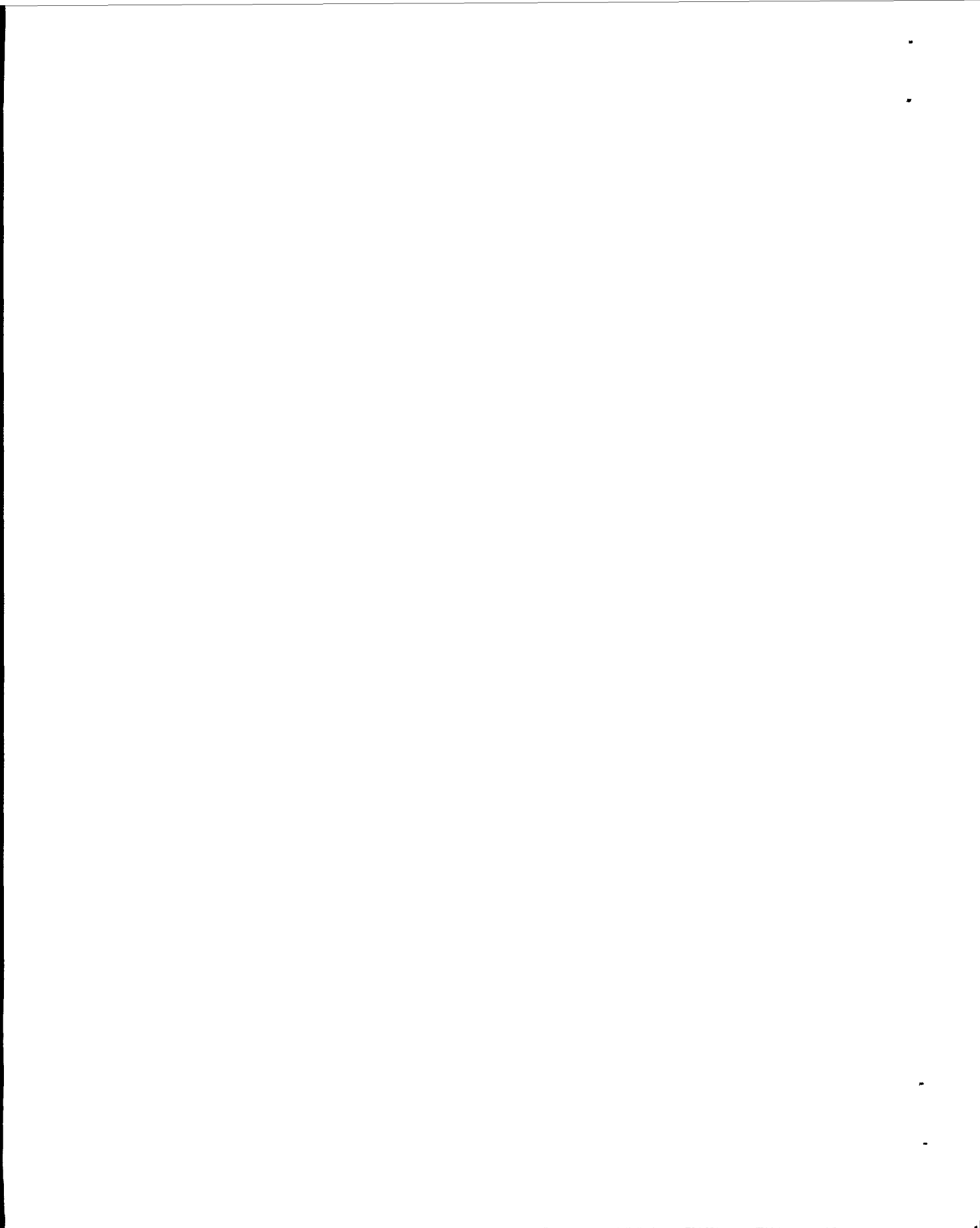


A - WATER DEPTH RATIOS AND GAS DENSITY RATIOS ACROSS BOW WAVE



B - RELATIVE ERROR INCURRED

Figure 2 - Static Depth and Density Ratios Across Oblique Wave as Function of Upstream Mach (Froude) Number



SECTION III - TEST FACILITY

1. TOW CHANNEL AND INSTRUMENTATION

Pertinent dimensions and characteristics of the shallow water tow channel at Wright-Patterson Air Force Base are:

1. Length - 45 ft
2. Width - 4 ft
3. Usable run length to test section - 26.3 ft
4. Side and end wall construction - metal
5. Bottom surface construction - four clear glass plates placed end to end, each 0.5 inches thick
6. Bottom surface support - 163 movable jack pads that can be adjusted to maintain the bottom surface level within 0.005 in. in a 4-ft by 4-ft area

The model was transported by a movable tow carriage that spanned the width of the channel and rode on a series of wheels supported by the structure on each side.

An instrumented console was electronically connected to the tow carriage for supplying the power input to move the carriage at a controlled velocity. The carriage velocity can be controlled to give a Froude number range (based on a water depth of 0.19 in.) of about 0 to 8 (at a water depth of 0.19 in., a carriage velocity of 0.714 fps corresponds to a Froude number value of 1). The desired test Froude number value was selected using a calibrated dial prior to the test run. An approximate in-test Froude number value can be read from a "Machometer" located on the console. An accurate determination of the actual Froude number through the test section also can be obtained immediately following each test from an output trace on light-sensitive paper by a Honeywell Model 1408 visicorder. An electronic signal is sent to the visicorder at 2-in. intervals all along the tow channel length. These signals are recorded as discrete pulses on the otherwise straight output trace. Timing lines also are recorded at a preset rate to enable the pulse frequency to be used to determine the carriage velocity.

2. PHOTOGRAPHIC EQUIPMENT

a. Sequence Still Camera

Still photographs were taken of the test model and surrounding flow field at the test section using a single camera equipped with a 35-mm wide-angle lens. The camera was attached to the movable tow carriage above

the test model (see Figure 3). The camera moved with the carriage and was tripped automatically at the test section to photograph the desired test results. With each test run and return of the carriage, the film in the camera automatically was advanced one frame, which made it ready immediately for another test. A counter also was electronically connected to the camera so that each test run and return of the carriage automatically upgraded the preceding number by one integer. Thus, an accurate count of the tests conducted was maintained.

Lighting for this type of photography was provided by two 500-w flood lamps, with one located on each side of the tow channel about one foot from the side walls and about two inches above the water surface. The light from each source passed through the water and glass bottom surface and was reflected back by a painted surface that ran the entire length of the tow channel beneath the glass plates. This oblique lighting produced a camera field of view that contained both highly illuminated and shadowed areas highlighting the wave patterns. The result was a two-dimensional picture similar in appearance to wind-tunnel schlieren photographs (see Appendix B).

This method of photography provided an easy and fast means of obtaining flow geometry data. By measuring attached bow wave angles or wave detachment distances, for example, the effects of changes in free-stream Froude number and body geometry also could be determined. Thus, this type of photography is useful for obtaining geometrical characteristics and determining data trends.

b. Stereophotogrammetric Camera/Projector Equipment

To study the quantitative aspects of the water-gas analogy, it was necessary to have available a method by which water depth data could be obtained. Such a method was provided by the stereo camera/projector.

In this method, two cameras were located on the movable tow carriage above the test model and were slightly off center of its centerline (see Figure 4). At the test section, each camera automatically and simultaneously photographed the test model and surrounding flow field, which produced two latent images of the same format area. These two-dimensional images were formed on photographically treated glass plates. After processing, the glass plates were inserted back into the cameras which, when used together as a projector system, produced an analogic, three-dimensional stereo model from the processed images.

From this stereo model, a water depth contour map was constructed (see Section V). This was accomplished using the camera/projector by passing a red light through the right stereo plate and a blue light through the left plate to form a common view area on a small circular tracing table. Special glasses (having a red lens and a blue lens) also were used. The tracing table was raised or lowered until a small pinpoint light source in the tracing table appeared to lie on a point on the water surface. Physically, this point and its height are defined when the same point in both

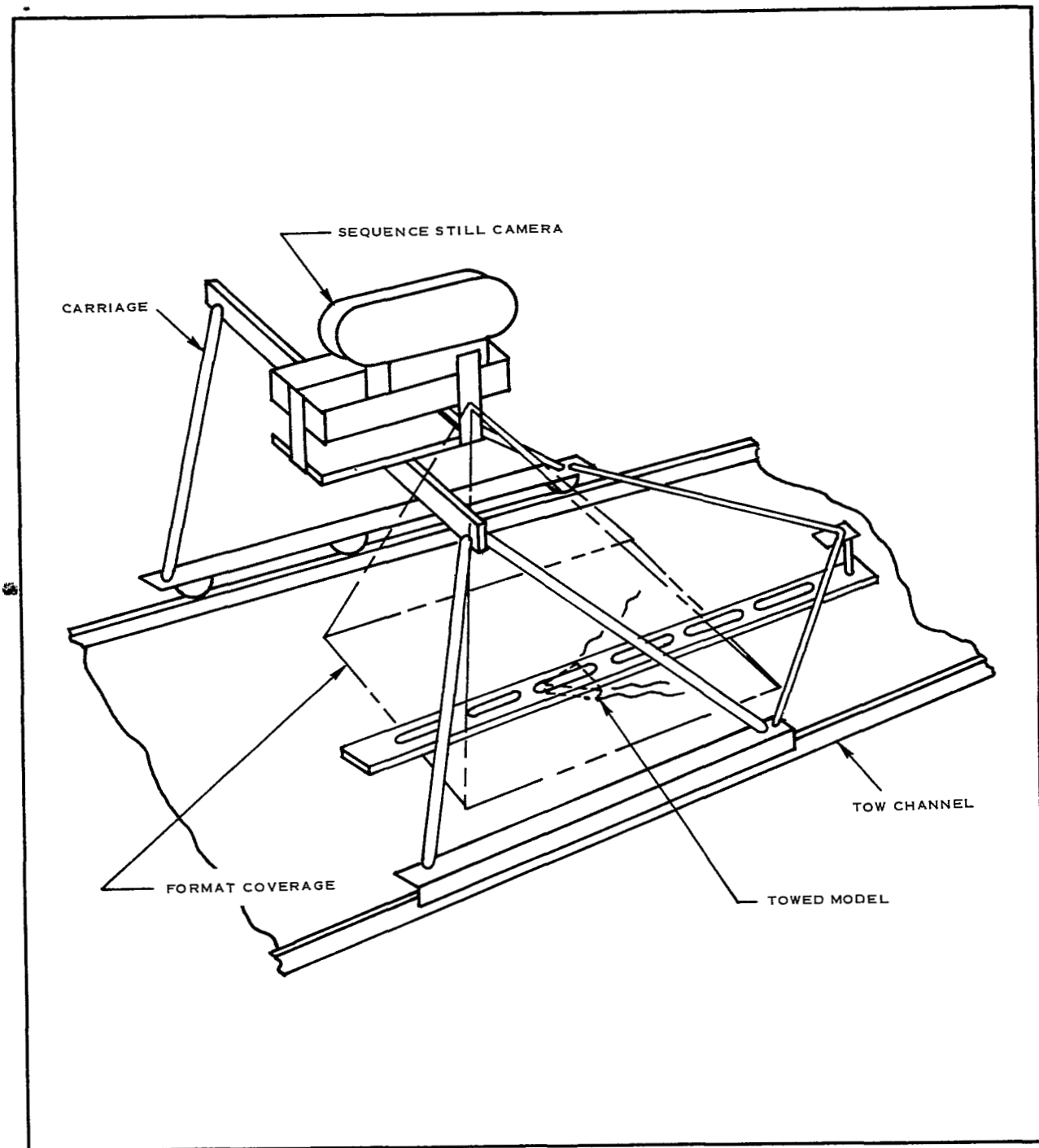


Figure 3 - Sequence Still Photographic Technique

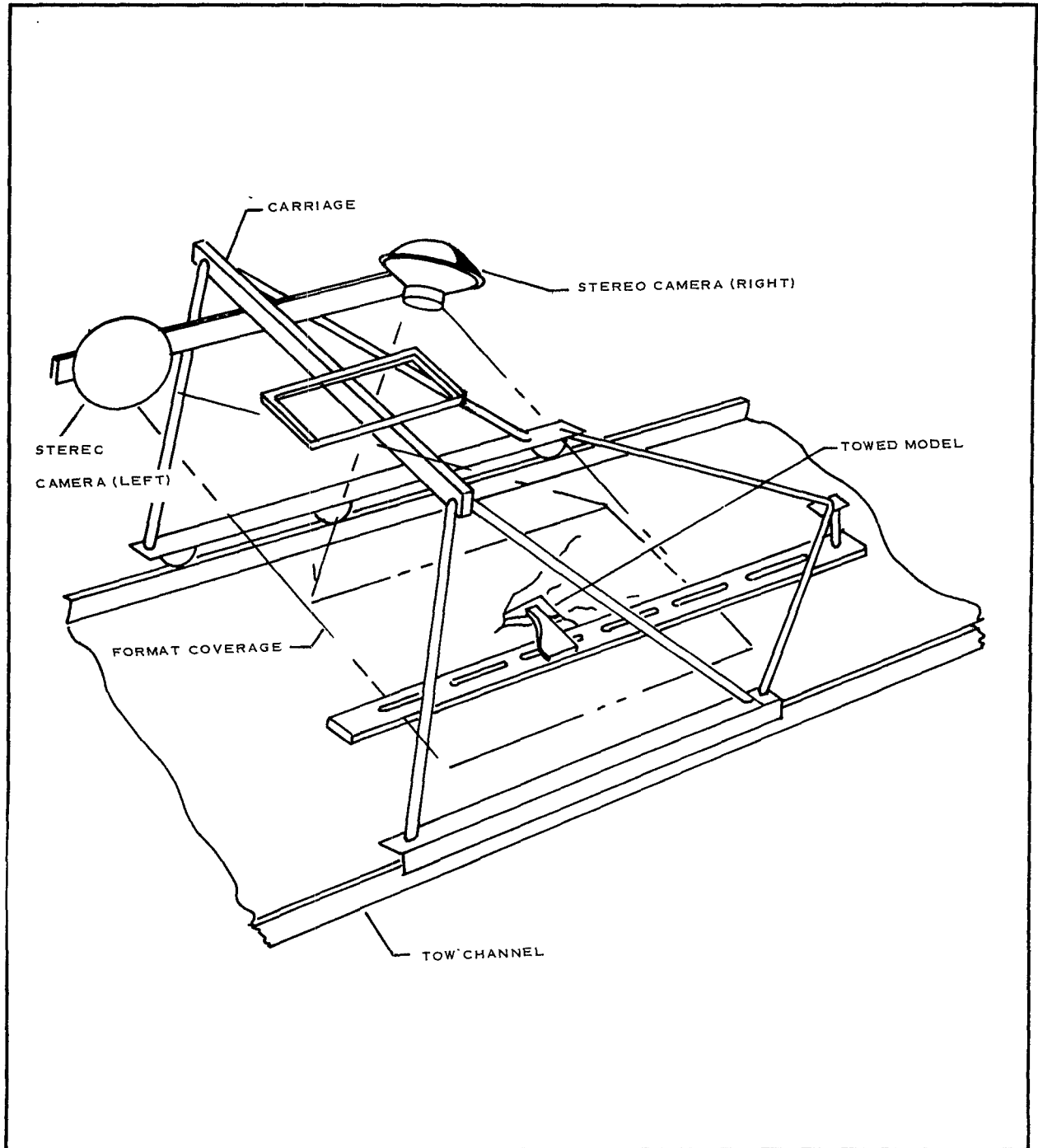


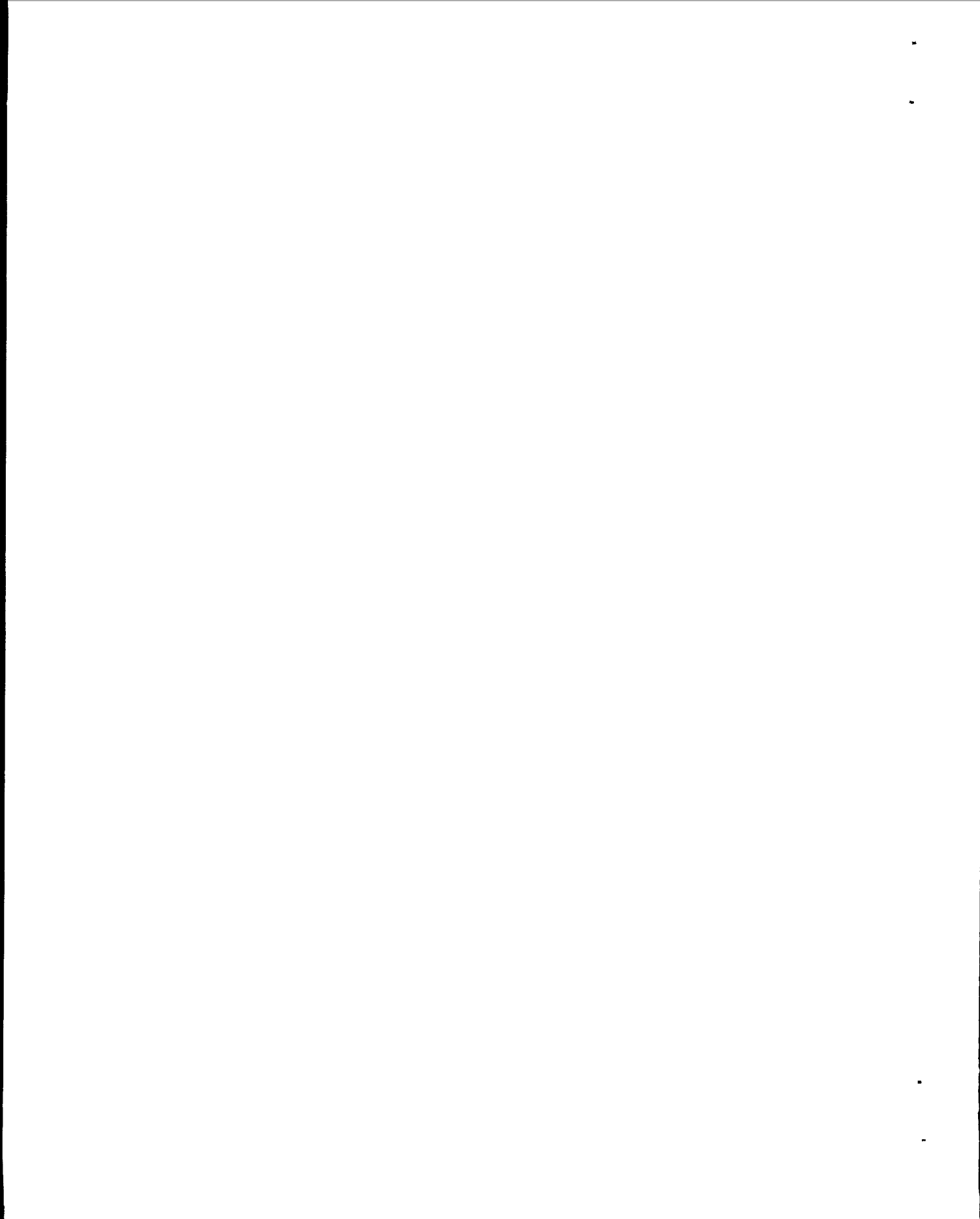
Figure 4 - Stereophotogrammetric Technique

images coincides. When this was achieved, the tracing table was moved to connect all adjacent points at the same height. This process then was repeated at various height levels until a complete contour map was formed.

Lighting for the stereo system was provided by an electronic strobe flash. Two units that flash simultaneously were used. These units were located on each side of the movable tow carriage about 18 in. above the water surface.

As a practical matter, it was necessary to use some material that facilitated the definition of the water surface during the reduction process. In this program, eccospheres (small white hollow spheres approximately six microns in diameter) were used. The particles floating on the water surface enabled its definition.

A small metal block exactly 0.5 in. in height also was placed in the test section for the stereo tests. This block provided a reference height from which the water depths could be determined.



SECTION IV - SUMMARY OF TEST RUNS AND CONDITIONS

1. DESCRIPTION OF TEST MODELS

The 58 two-dimensional body shapes used in the tow-channel test program are described in Table III. Although these models are representative of a wide variety of different geometrical shapes, it can be seen from Table III that they can be classified into 10 basic categories. Consequently, these models permitted the evaluation of the effects of individual geometric parameters.

2. SUMMARY OF TESTS

Tests performed and test conditions are summarized in Tables IV and V. In each table, the tests are classified according to the type of trailing body used or as single body tests. The analytical wedge and the analytical blunt body listed under the heading "Trailing Body" are a 10-deg-apex wedge and a reversed (backward-facing) half cylinder, respectively. These bodies were used as analytical aids in predicting wake Froude number profiles (see Section II, Volume I). As indicated by Tables IV and V, photographic data on selected two-body combinations also were obtained.

3. EXPERIMENTAL PROCEDURE

Sequence still data was obtained using the following basic procedure:

1. Film was loaded in camera and camera was placed in position on movable tow carriage. (Once this was accomplished, up to 700 tests could be conducted without removal of the camera).
2. Models were located and attached to the tow carriage.
3. Water depth was checked and water was added as required. (Static water depth was obtained to within 0.003 inches with the use of a vernier micrometer depth gage). Depth readings generally were not required prior to each run.
4. Carriage velocity control was set for the desired velocity.
5. Carriage motion was activated.

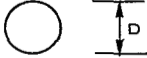

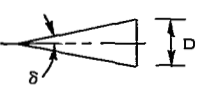

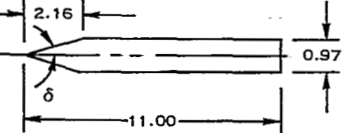
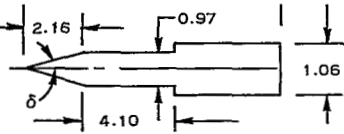
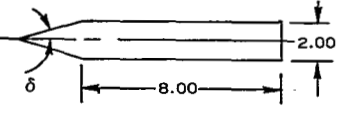
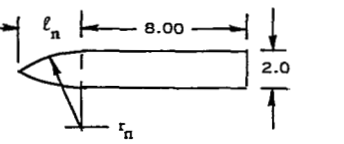
For stereo photography the basic procedures was as follows:

1. Photographic glass plates were placed into two special plate holders, which then were inserted into the two cameras.

2. Models were located and attached to the tow carriage.
3. Water surface definition material was dispensed as required and reference gage block was positioned.
4. Static water depth was checked and water was added as required (the same method used for sequence still photography was used for the stereo photography. The stereo results themselves, however, provided a second check.)
5. Shutters (spring loaded) on each stereo camera were cocked so that the shutters would open at the test section.
6. The carriage velocity control was set for the desired velocity.
7. Carriage motion was activated.
8. At the conclusion of each test, the plate holders were removed from each camera and the exposed glass plates were removed from the plate holders.

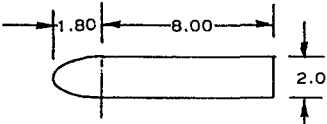
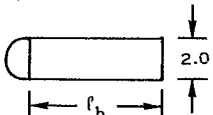
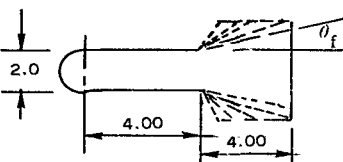
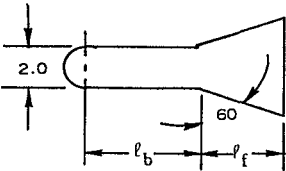
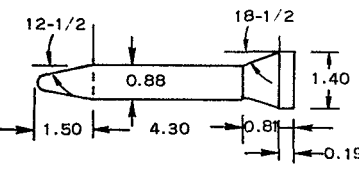
In general, time required to conduct a single stereo test was an order of magnitude higher than the time required to conduct a single sequence still test.

TABLE III - TEST CONFIGURATIONS

Classification	Number of configurations	Design variables*
Circular cylinder 	3	D = 1, 2, and 4
Half cylinder 	2	D = 2 and 4
Sharp wedge 	17	D = 1; 2δ = 10 D = 2; 2δ = 15, 20, 30, 60, 80, 100, and 110 D = 4; 2δ = 30, 40, 45, 50, 55, and 60
Blunted wedge (80- and 120-deg apex angle) 	13	D = 2, 2δ = 120, r _s /R = 0.40, r _n /R = .0.25 D = 2, 2δ = 120, r _s /R = 0.20, r _n /R = 0.25 D = 2, 2δ = 120, r _s /R = 0.00, r _n /R = 0.25 D = 4, 2δ = 80 and 120, r _s /R = 0.00, r _n /R = 0.25 D = 4, 2δ = 80 and 120, r _s /R = 0.05, r _n /R = 0.25 D = 4, 2δ = 80 and 120, r _s /R = 0.10, r _n /R = 0.25 D = 4, 2δ = 80 and 120, r _s /R = 0.20, r _n /R = 0.25 D = 4, 2δ = 80 and 120, r _s /R = 0.30, r _n /R = 0.25
Wedge-block 	1	δ = 12.66,
	1	δ = 12.66
	2	2δ = 30 and 60
Ogive-block 	3	l _n = 4.0, r _n = 8.5; l _n = 6.0, r _n = 18.5; and l _n = 8.0, r _n = 32.5

* Dimensions in inches, angles in degrees.

TABLE III - TEST CONFIGURATIONS (Continued)

Classification	Number of configurations	Design variables *
<p>Parabolic nose-block</p> 	1	
<p>Half cylinder-block</p> 	4	$l_b = 2.0, 4.0, 6.0, \text{ and } 8.0$
<p>Half cylinder-block-flare</p> 	5	$\theta_f = 15, 20, 30, 45, \text{ and } 60$
	5	$l_b = 7.0, l_f = 2.0; l_b = 6.5, l_f = 2.5; l_b = 6.0, l_f = 3.0; l_b = 5.5, l_f = 3.5; l_b = 5.0, l_f = 4.0$
<p>Blunted wedge-block-flare</p> 	1	...

*Dimensions in inches, angles in degrees.

TABLE IV - TOW CHANNEL TEST SUMMARY
(SEQUENCE STILL PHOTOGRAPHIC TECHNIQUES)

Forebody class	Forebody diameter (in.)	Trailing body*	Separation distance range, x/D	Number of tests	Primary test purpose
Circular cylinder	1, 2, 4	None	NA [†]	21	Flow geometry
		Analytical blunt body	. . .	0	. . .
	1, 2, 4	Analytical wedge	4, 5	11	Wake survey
		Others	. . .	0	. . .
Half cylinder	2, 4	None	NA	27 [‡]	Flow geometry, wave standoff
	2, 4	Analytical blunt body	4 to 10.5	10	Wake survey
	2, 4	Analytical wedge	4 to 10.5	3	Wake survey
	2, 4	Others	6 to 10	20	Two-body flow geometry
Sharp wedges	1, 2, 4	None	NA	42	Flow geometry
	2, 4	Analytical blunt body	4 to 12.5	28	Wake survey
	2, 4	Analytical wedge	4 to 12.5	20	Wake survey
		Others	6 to 10	39	Two-body flow geometry
Blunted 80- and 120-deg wedges	2, 4	None	NA	6 [§]	Flow geometry
	2, 4	Analytical blunt body	4 to 12.5	74	Wake survey
	2, 4	Analytical wedge	2 to 12.5	48	Wake survey
	2, 4	Others	4 to 10	165	Two-body flow geometry
Wedge-block	1, 2	None	NA	3	Flow geometry
	1	Analytical blunt body	2 to 19	45	Wake survey
	1	Analytical wedge	4 to 12	65	Wake survey
	1	Others	4 to 10	159	Two-body flow geometry
Ogive-block	2	None	NA	3 [§]	Flow geometry
Parabolic nose-block	2	None	NA	3	Flow geometry
Half cylinder-block	2	Analytical blunt body	6.5 to 12.5	9	Wake survey
		Analytical wedge	6 to 10	12	Flow geometry, wake survey
		Others	4 to 6	18	Two-body flow geometry
Half cylinder-block-flare	4, 4 ~ 6	None	NA	9	Flow geometry
		Analytical blunt body	4 to 6.25	18	Wake survey
		Analytical wedge	3 to 5	31	Wake survey
		Others	4, 6	19	Two-body flow geometry
Blunted wedge-block-flare	1.4	None	NA	6	Flow geometry
		Analytical blunt body	9.6 to 16.4	9	Wake survey
		Analytical wedge	6 to 12	9	Wake survey

Note: Froude number range: 1.5 to 2.5.

*Analytical blunt body = reversed half cylinder; analytical wedge = 10-deg wedge; others = circular cylinder, half cylinder, sharp wedges, blunted 80-deg wedges.

[†]Not applicable.

[‡]Includes three tests of reversed half cylinder.

[§]Includes 27 tests with forebody at angles of attack 5, 15, and 25 deg.

TABLE V - TOW-CHANNEL TEST SUMMARY (STEREO PHOTOGRAPHIC TECHNIQUES)

Forebody classification	Forebody diameter (in.)	Trailing body	Freestream Froude number, Fr_{∞}	Separation distance range, x/D	Primary test purpose
Circular cylinder	2, 4	None Others*	1.5, 2.0, 2.5 2.0	NA ⁺ 6 to 10	Flow investigation Two-body flow analysis
Half cylinder	2, 4	None Sharp wedge	1.5, 2.0, 2.5	NA 6 to 10	Flow investigation Two-body flow analysis
Sharp wedge	1, 2, 4 2, 4	None Analytical wedge	1.5, 2.0, 2.5 1.5, 2.0, 2.5	NA 6 to 10	Flow investigation Wake profiles
Blunted 80- and 120-deg wedge [‡]	2, 4	None	1.5, 2.0, 2.5	NA	Flow investigation
	2, 4	Analytical blunt body	1.5, 2.0 to 2.5	4 to 17	Wake profiles
		Analytical wedge Others	1.5, 2.0, 2.5 1.5, 2.0, 2.5	3 to 10 4 to 10	Wake profiles Two-body flow analysis
Wedge-block [§]	1	None	1.5, 2.0, 2.5	NA	Flow analysis
	1	Analytical blunt body	1.5, 2.0, 2.5	4 to 17	Wake profiles
	1	Analytical wedge	1.5, 2.0, 2.5	3 to 8	Wake profiles
	1	Other	2.0	4 to 10	Two-body flow analysis
Blunted wedge-block-flare	1.4	None	1.5, 2.0, 2.5	NA	Flow investigation
	1.4	Analytical blunt body	1.5, 2.0 to 2.5	6.6 to 16.4	Wake profiles
	1.4	Analytical wedge	1.5, 2.0, 2.5	4 to 10	Wake profiles Two-body flow analysis

*Analytical blunt body = reversed half cylinder; analytical wedge = 10-deg wedge; others = circular cylinder, half cylinder, sharp wedges, and blunted 80-deg wedge.

⁺Not applicable.

[‡]Tests performed included 32 tests with 120-deg wedge at angles of attack 5, 15, and 25 deg.

[§]Tests performed include 39 tests with wedge-block at angles of attack 5, 15, and 25 deg.

SECTION V - RESULTS

1. SEQUENCE STILL DATA

a. Data Trends

Pertinent tow-channel data trends and results are presented in Figures 5 through 12 as a function primarily of free stream Froude number, Fr_{∞} . It can be seen that, in general, with an increase in free stream Froude number:

1. Bow wave standoff parameter, S/D , decreases
2. Approximate wake neck location, x_o/D , increases
3. Trailing wake divergence half angle, ϵ , (similar to the recompression shock half angle in a gas), decreases.

These trends are similar to those that would be expected from applicable theory or wind-tunnel results. Other independent parameters that produce more or less expected trends for specific models include deflection angle (wedge apex half angle), flare angle, wedge shoulder radius, flare size, and nose geometry. At constant Mach number, for example, an increase in apex angle causes a general increase in S/D and x_o/D (Figure 6). This trend is quite pronounced for these parameters as would be expected due to the increased bluntness. It is less pronounced, although still apparent, for ϵ where the higher deflection angle causes a reduced Mach number flow along the sides and thus promotes a larger flow turning angle as the flow leaves the wedge.

The flare angle and flare length both show comparatively minor effects except in some isolated cases (see Figures 10 and 11). These results are generally as expected and consistent with other applicable trends. Shoulder radius effects are almost nonexistent forward of the body as might be expected, but are somewhat more pronounced on those parameters measured aft of the body; particularly x_o/D (Figure 7). The trend here again, however, is predictable since smaller x_o/D values might be associated with larger shoulder radius. Finally, the nose shape effects (see Figures 8 and 12) are generally as expected.

Some interesting aspects of this data can be observed from Figures 5, 6, and 10. From Figure 6, it can be seen that at $Fr_{\infty} = 1.5$ and $\delta > 25$ deg, a pronounced difference in S/D is obtained for the two model sizes shown. This is attributed to wall effects, which influenced both the shape and location of the bow wave for the larger model. At $Fr_{\infty} = 1.5$, Figure 10 shows a comparatively large increase in S/D . The flare length (and thus the diameter) increases. This possibly results from the flare size becoming the dominant factor influencing the location and shape of the bow

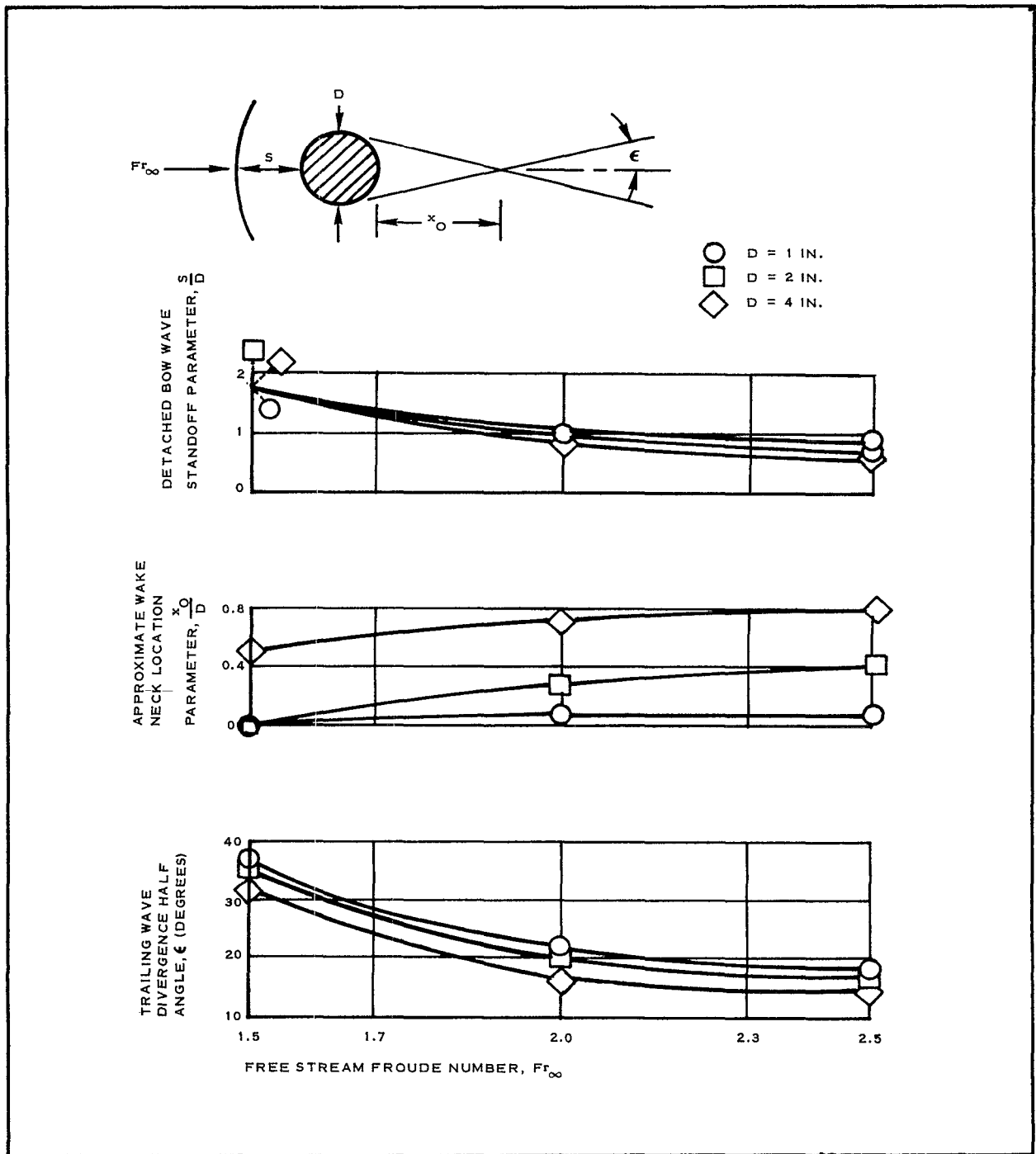


Figure 5 - Effects of Free-Stream Froude Number on Circular Cylinder Data

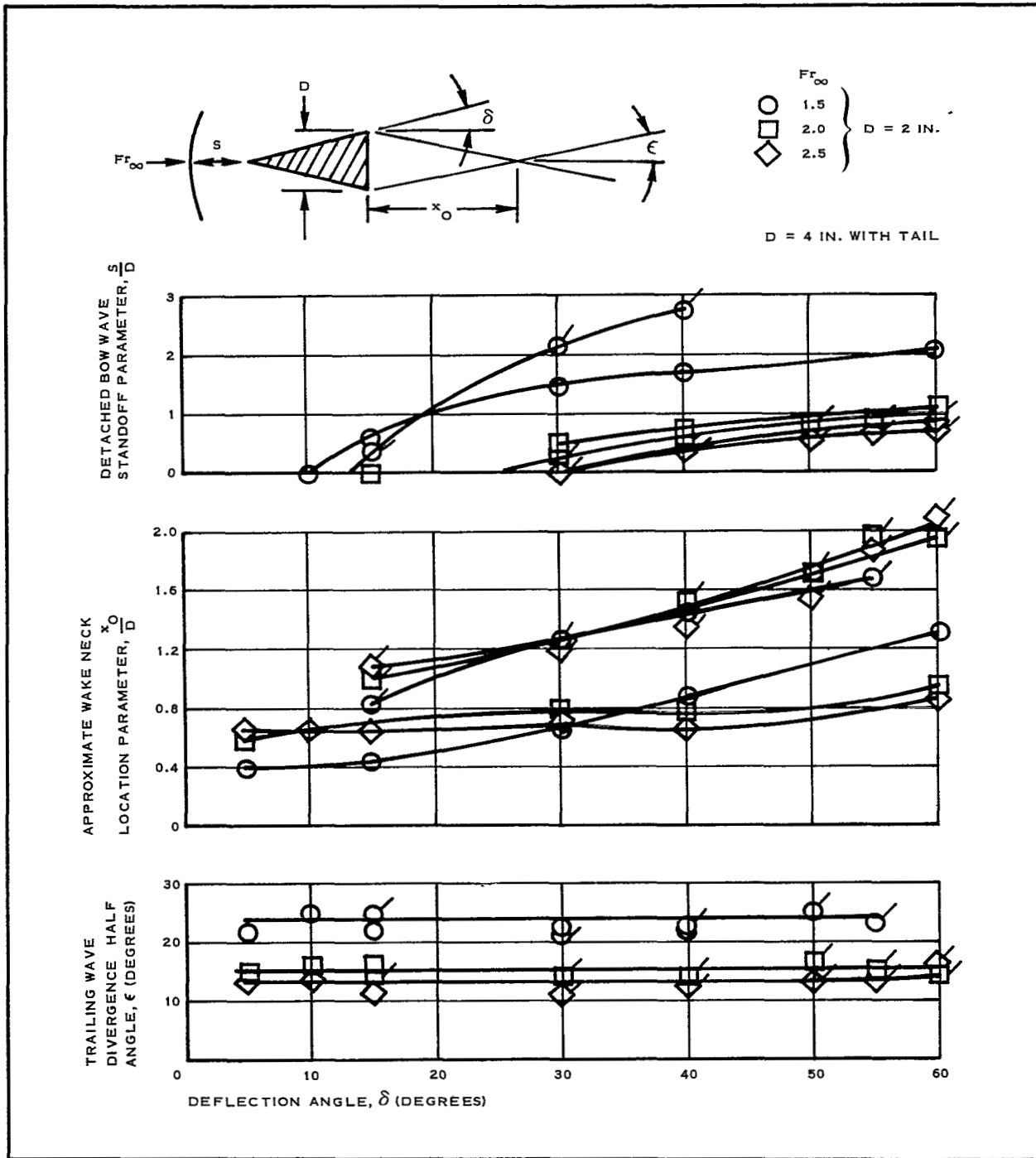


Figure 6 - Effects of Deflection Angle and Model Size on Wedge Data

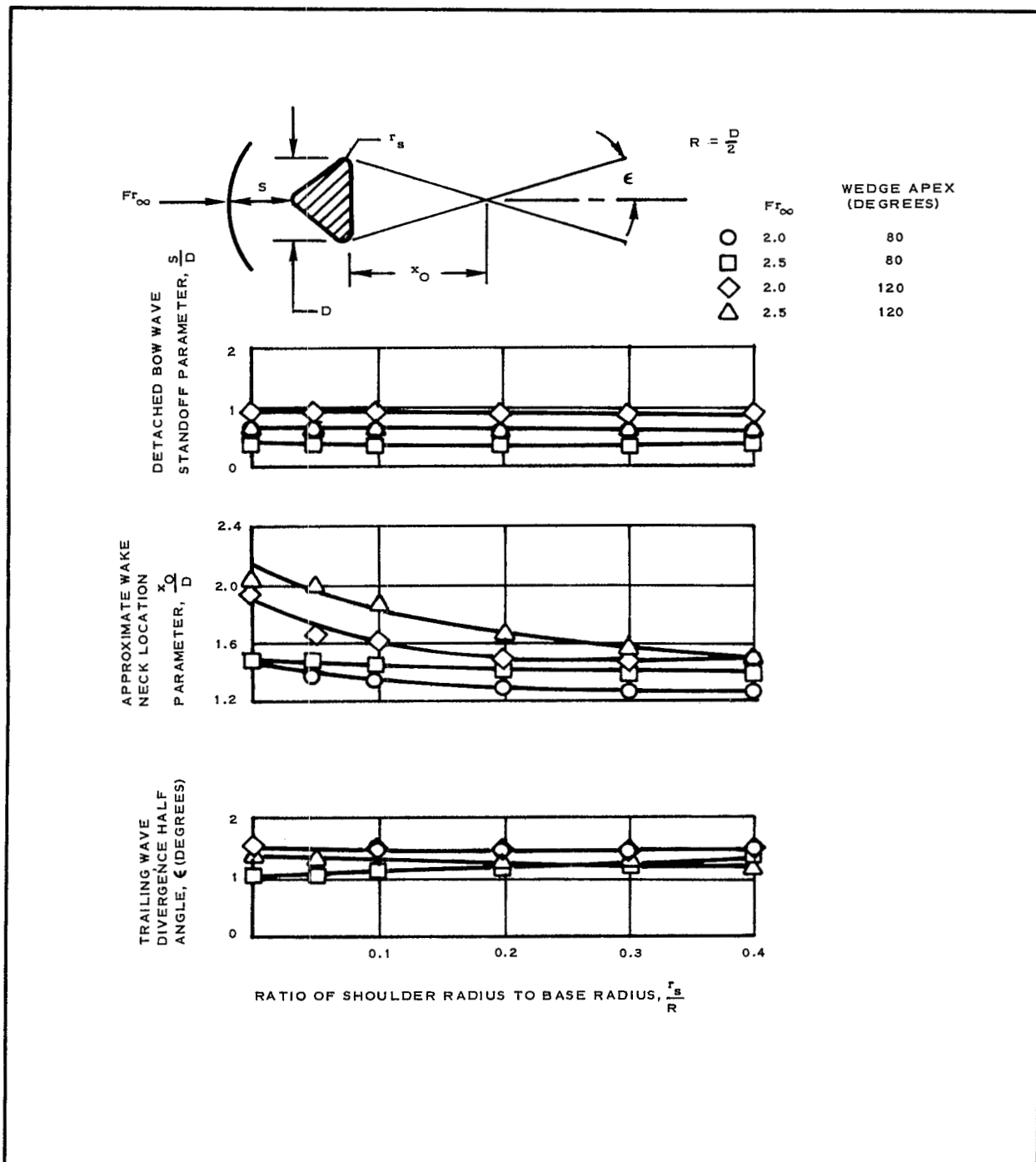


Figure 7 - Effects of Shoulder Radius on a 80- and 120-Degree Wedge Data

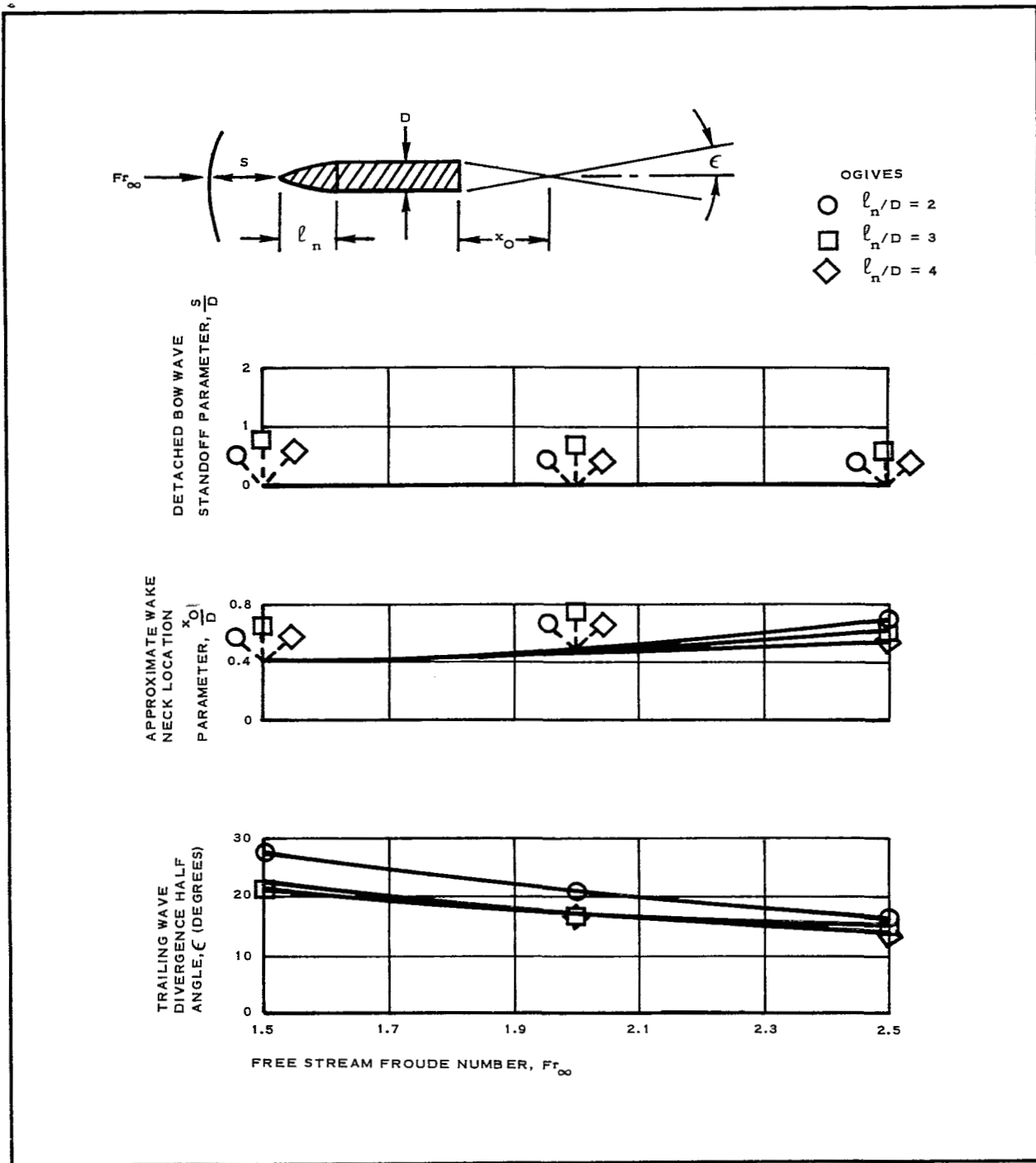


Figure 8 - Effects of Free-Stream Froude Number on Ogive-Block Configuration

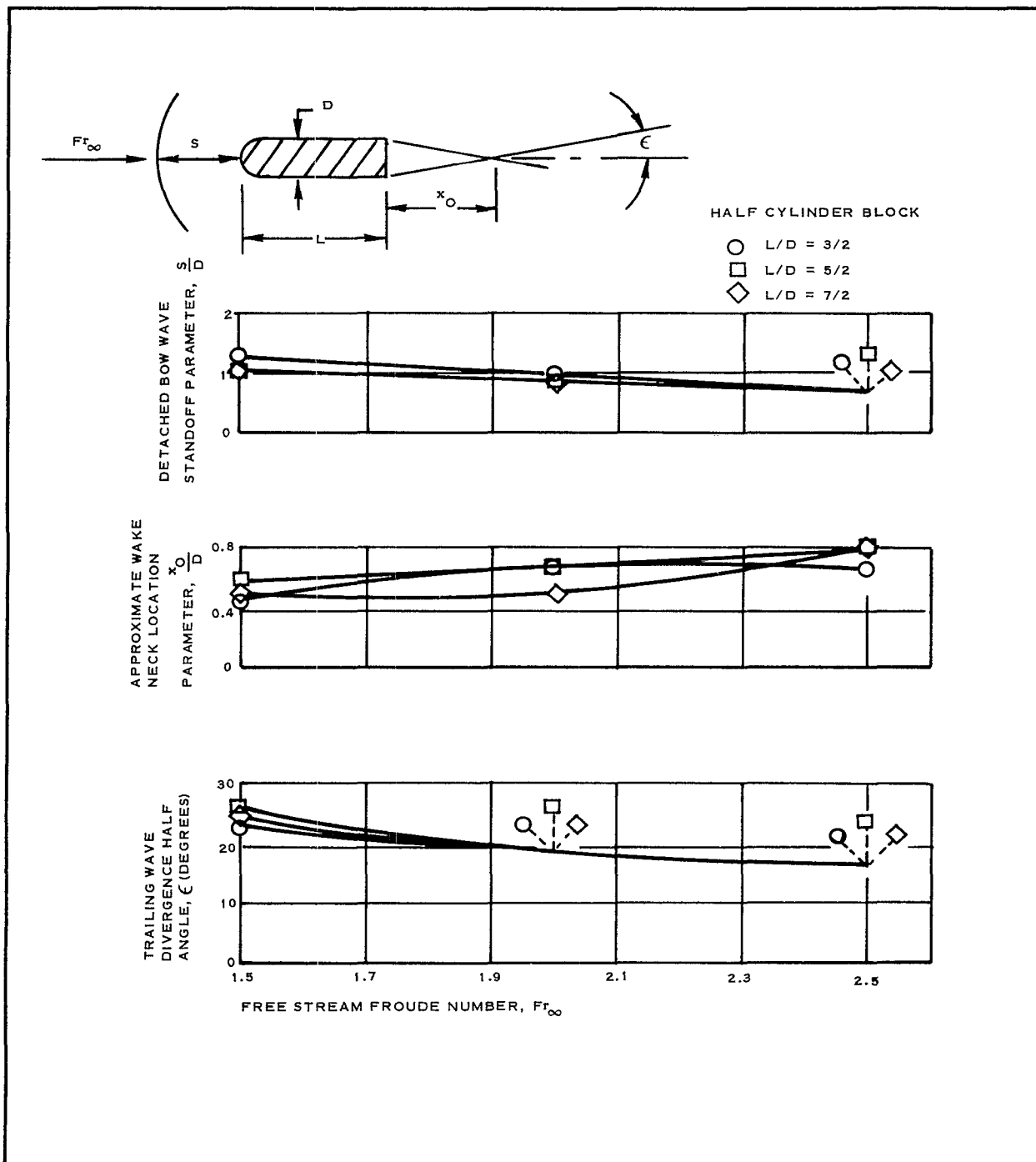


Figure 9 - Effects of Free-Stream Froude Number on Half Cylinder-Block Configurations

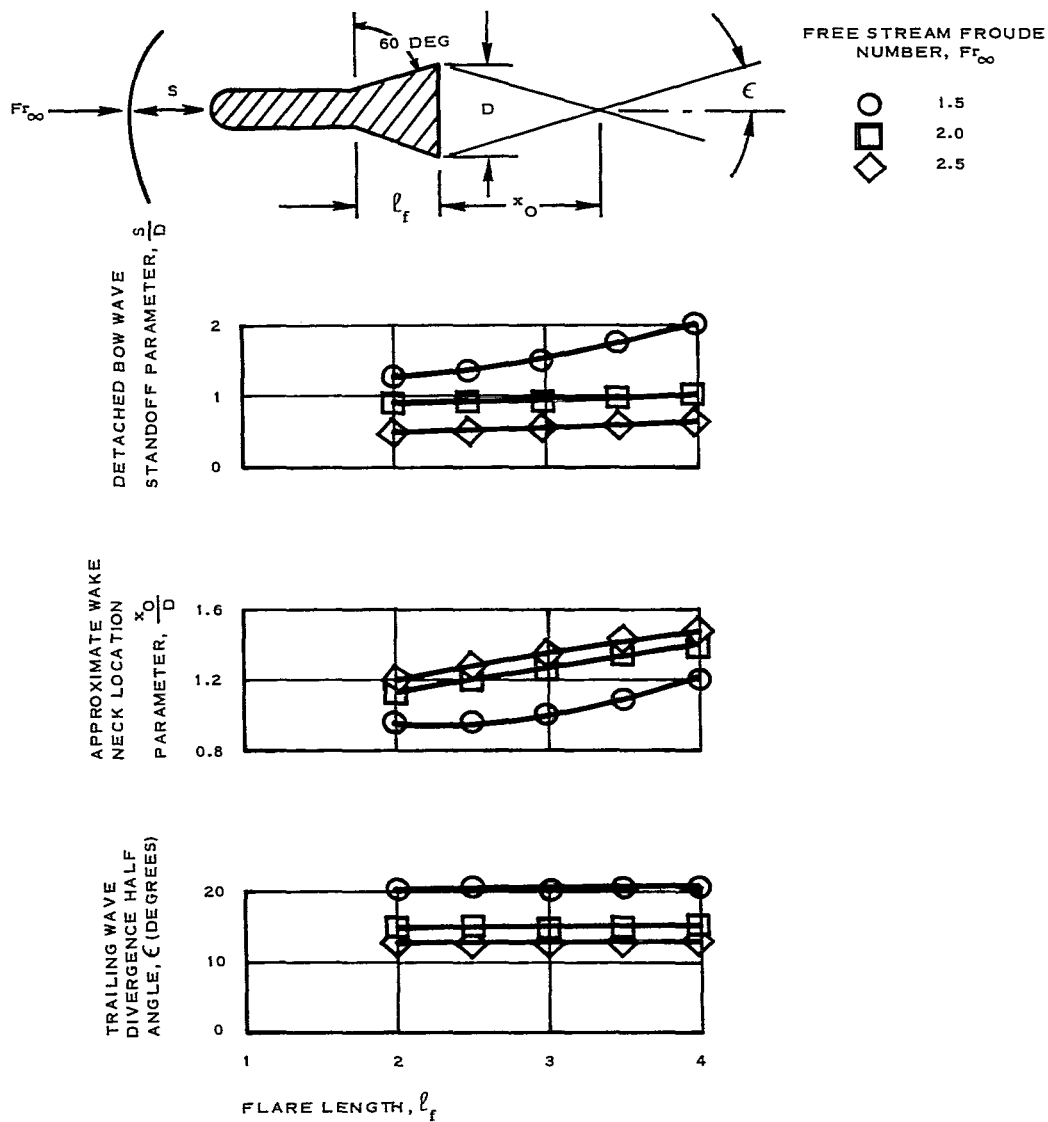


Figure 10 - Effects of Flare Length on Half Cylinder-Block-Flare Configurations

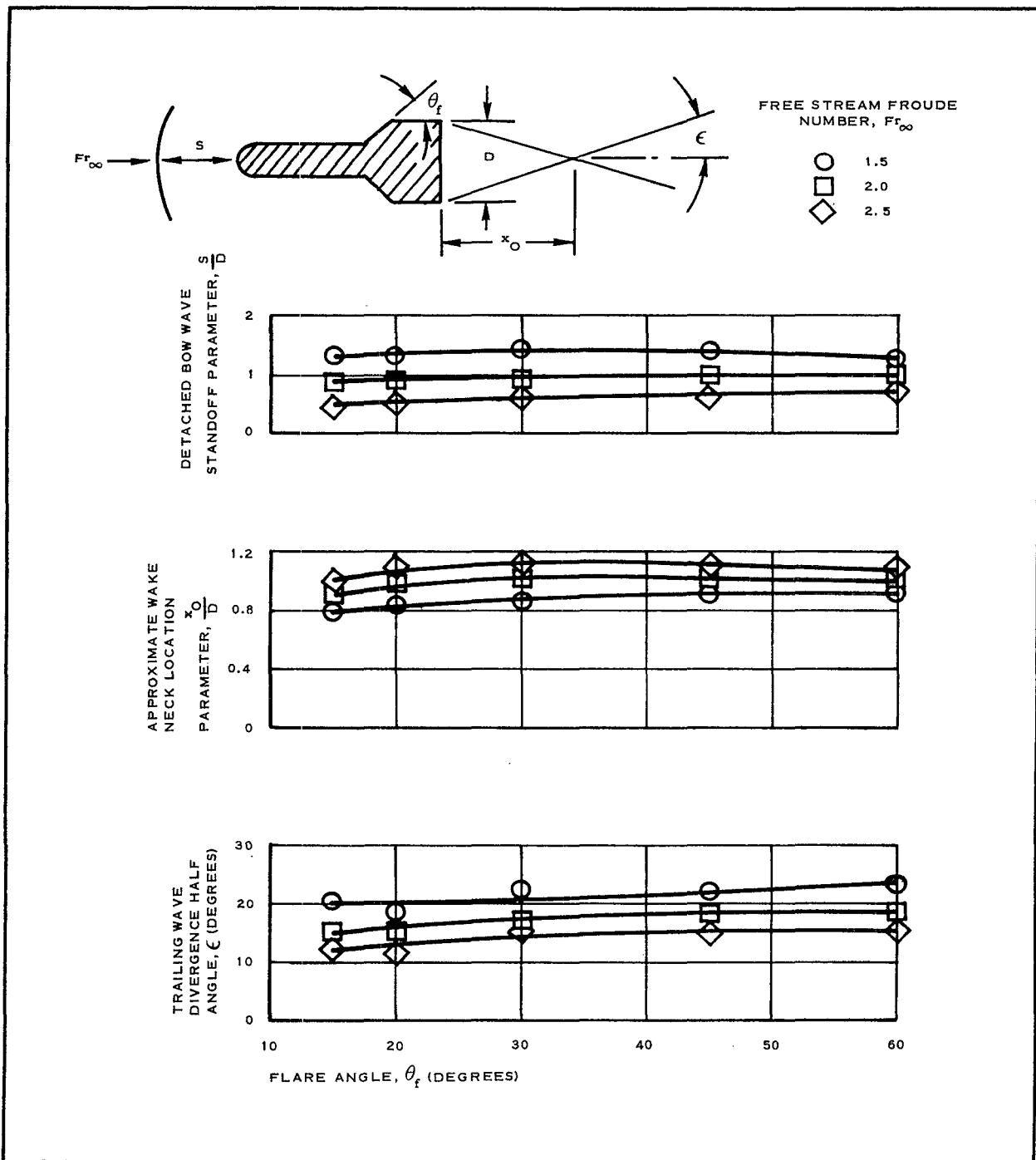


Figure 11 - Effects of Flare Angle on Half Cylinder-Block-Flare Configurations

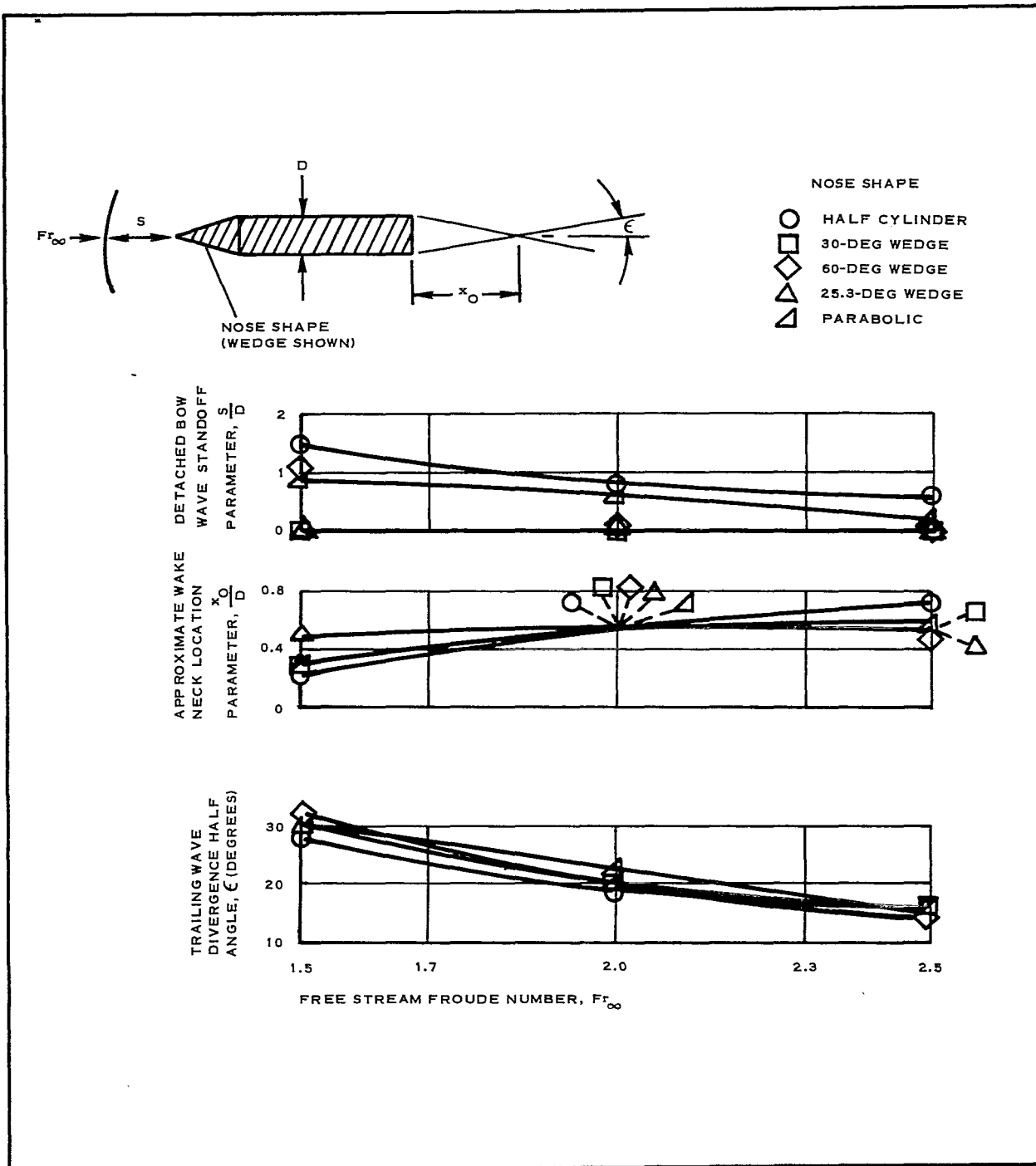


Figure 12 - Effects of Free-Stream Froude Number and Nose Geometry on Block Configuration with Different Nose Shapes

wave, although, again, wall effects may be influencing the data. Finally, both Figures 5 and 6 show a model size effect on x_0/D . This is somewhat contrary to what would be expected in a gas flow and results from the tendency of the water flow to follow the contours of a body even around sharp base corners. The low actual boundary-layer velocities and surface tension in the water are considered to be the reason for this tendency. Percentage-wise, the smaller models are the most affected with separation occurring near and at the base centerline. Consequently, the x_0/D values for the larger models are considered to be more indicative of two-dimensional gas flow results.

b. Angle-of-Attack Effects on the Hydraulic Jump

Data presented in Section II, Volume I show the effects of towing a wedge block and a 120-deg wedge at angle-of-attack, α , values. These data show that the downstream surface produces a more oblique wave than the upstream surface as long as the wave remains attached. These results are consistent with oblique shock theory since the effective deflection angle on the upstream side is less than that on the downstream side. Data for the 120-deg wedge, for which the hydraulic jump is detached, show that the bow wave standoff parameter, S/D , decreases with increasing α for $\alpha > 5$ deg. This is attributed to a decrease in the effective frontal size of the model.

c. Comparison of Hydraulic Jump and Theoretical Gas Shock Results

Theoretical gas and tow channel attached two-dimensional bow wave results are shown in Figures 13 and 14. It is apparent from these figures that the hydraulic jump conforms reasonably well with theory for a $\gamma = 2$ gas. The best agreement is achieved for the two cases where the deflection angle, δ , is 5 deg. It also can be observed for these cases that the theory is nearly independent of γ . At larger deflection angles, some curvature is indicated by the data points; although, near the apex, the tow channel data agrees well with the $\gamma = 2$ theory. The indicated curvature of the data is consistent with real-gas results as the wave would be expected eventually to become a Mach line.

A comparison is made in Section IV of Volume I between detached hydraulic jump data from the tow channel and theoretical shock shape and location results for two-dimensional gases (air and a $\gamma = 2$ gas). The results indicate that the hydraulic jumps do not correspond to either the air or the $\gamma = 2$ gas theoretical results particularly in standoff distance. Good agreement between modified hydraulic jump data and axisymmetric shock shapes was found to exist for limited but diverse body geometries.

2. STEREO DATA

Representative results obtained using the stereophotogrammetric equipment are presented in Figures 15, 16, and 17 in the form of contour maps for the bodies indicated. The numbers represent the water depths obtained from a calibrated gage and indicate the relative height of the tracing table.

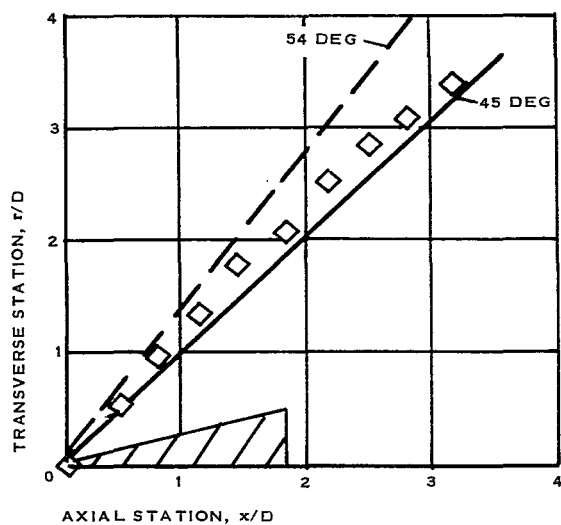
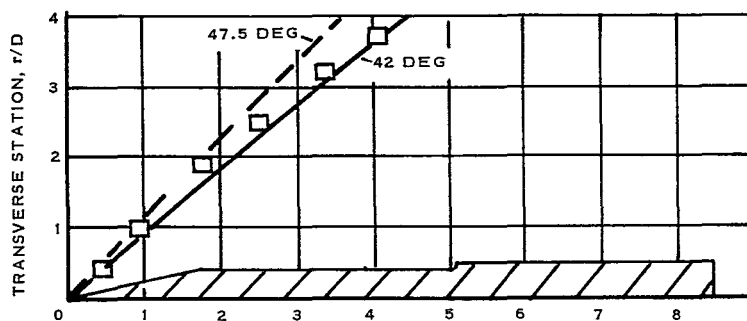
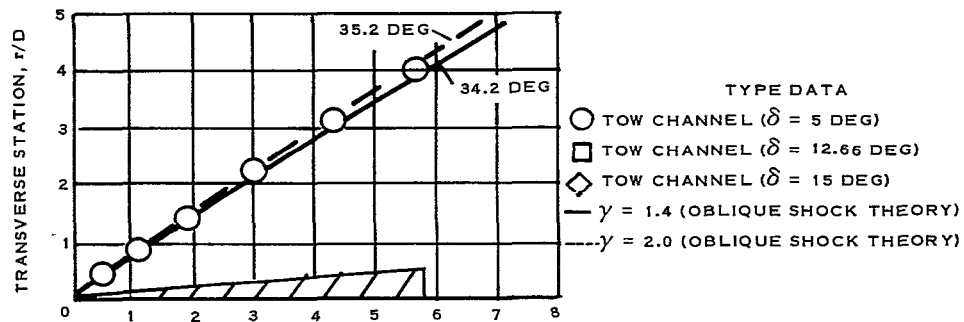


Figure 13 - Comparison of Attached Hydraulic Jump Geometry with Oblique Shock Theory at Mach (Froude) Number of 2

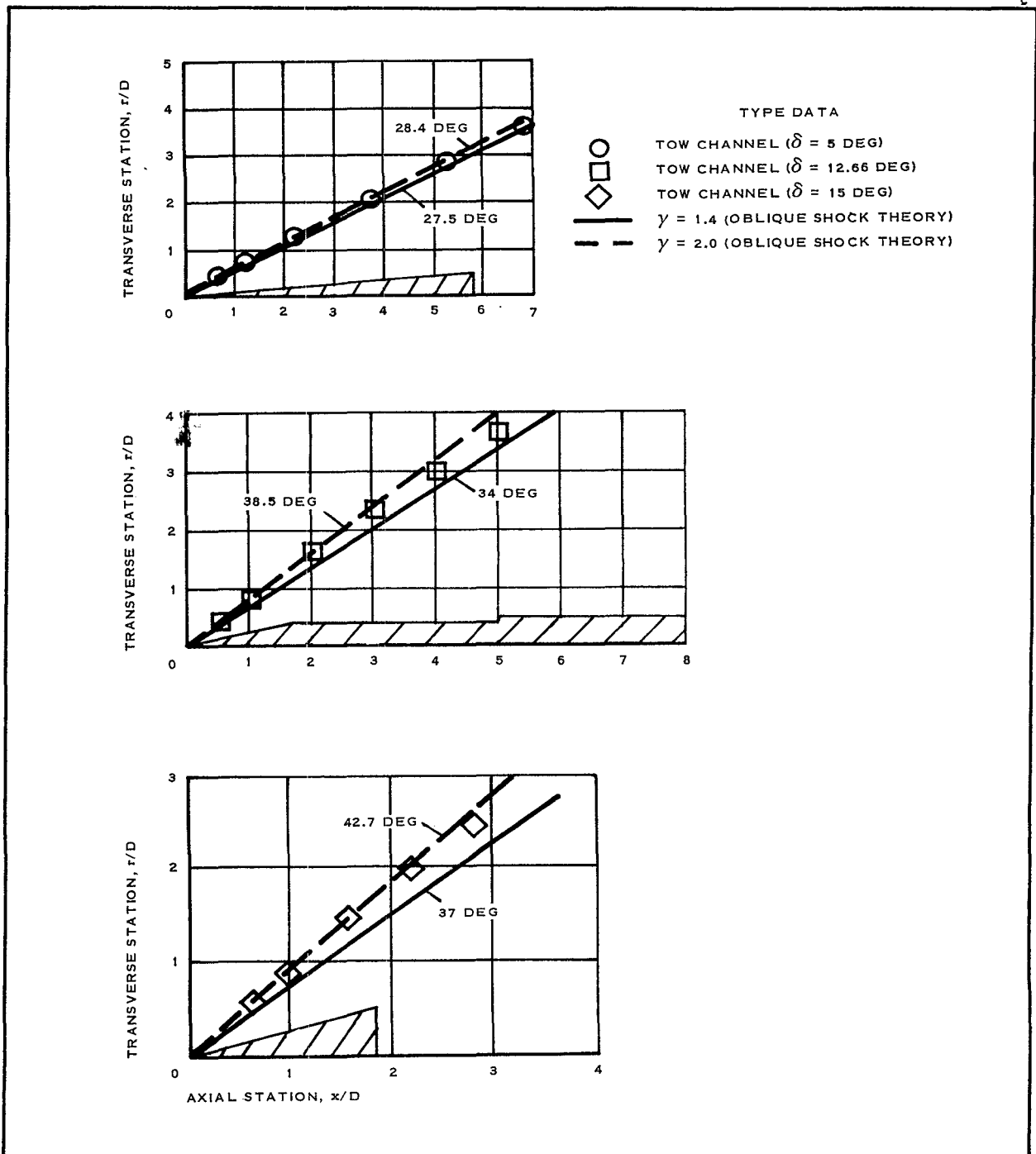


Figure 14 - Comparison of Attached Hydraulic Jump Geometry with Oblique Shock Theory at Mach (Froude) Number of 2.5

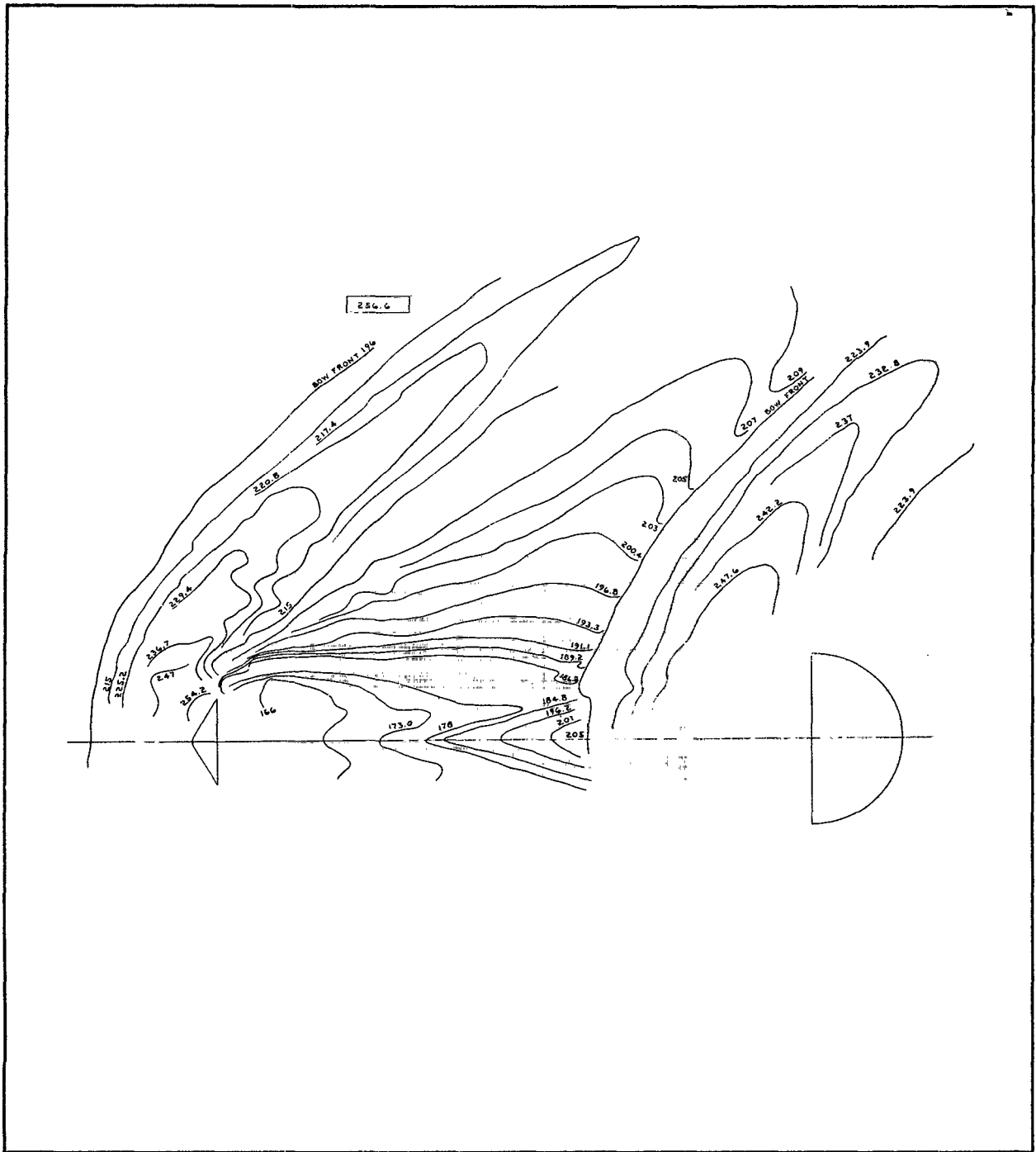


Figure 16 - Stereo Contour Map at $Fr_{\infty} = 2.2$ (120-Deg Wedge Forebody and Reversed Half Cylinder Trailing Body)

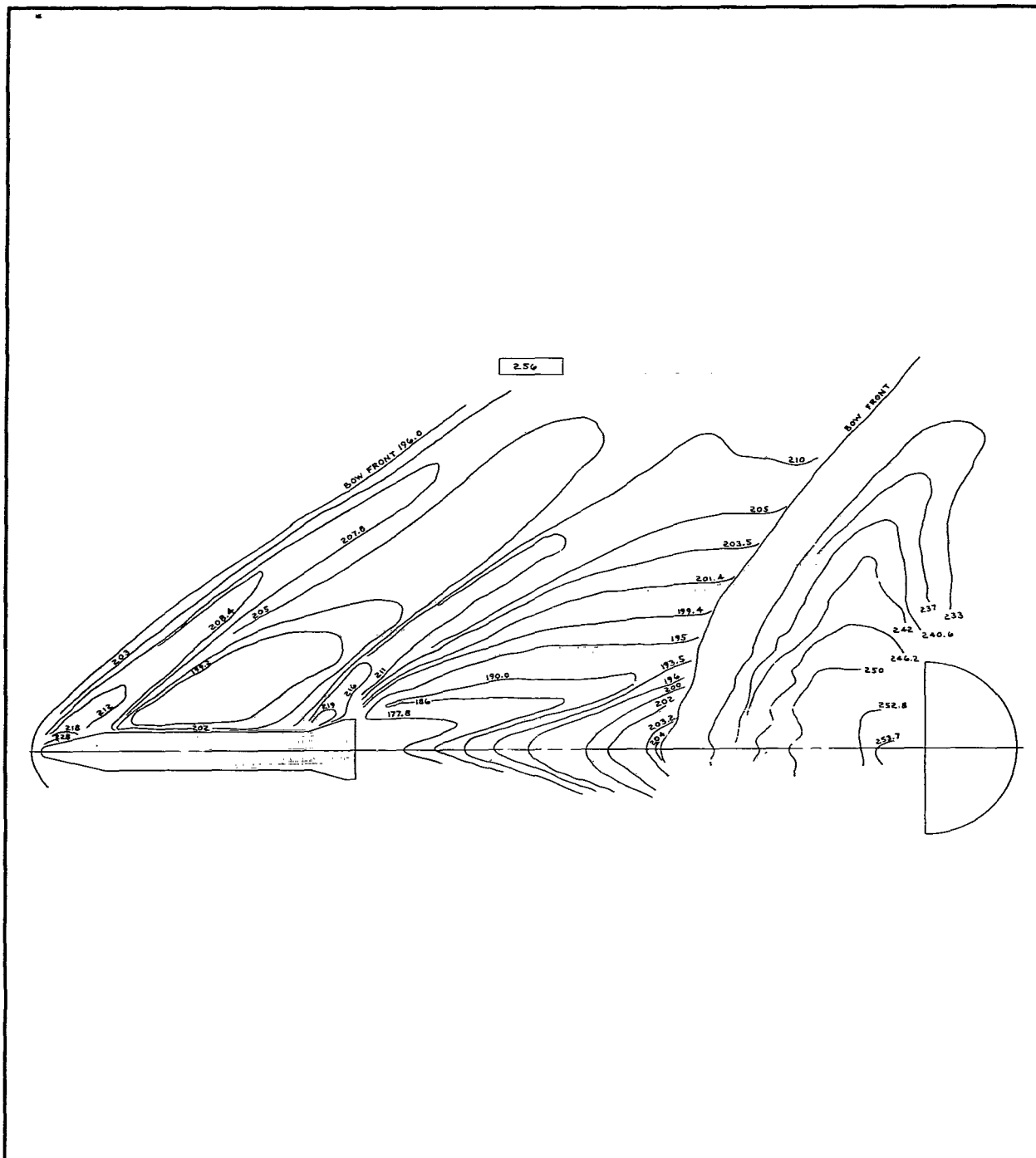


Figure 17 - Stereo Contour Map at $Fr_{\infty} = 2.2$ (Blunted Wedge Block-Flare Forebody and Reversed Half Cylinder Trailing Body)

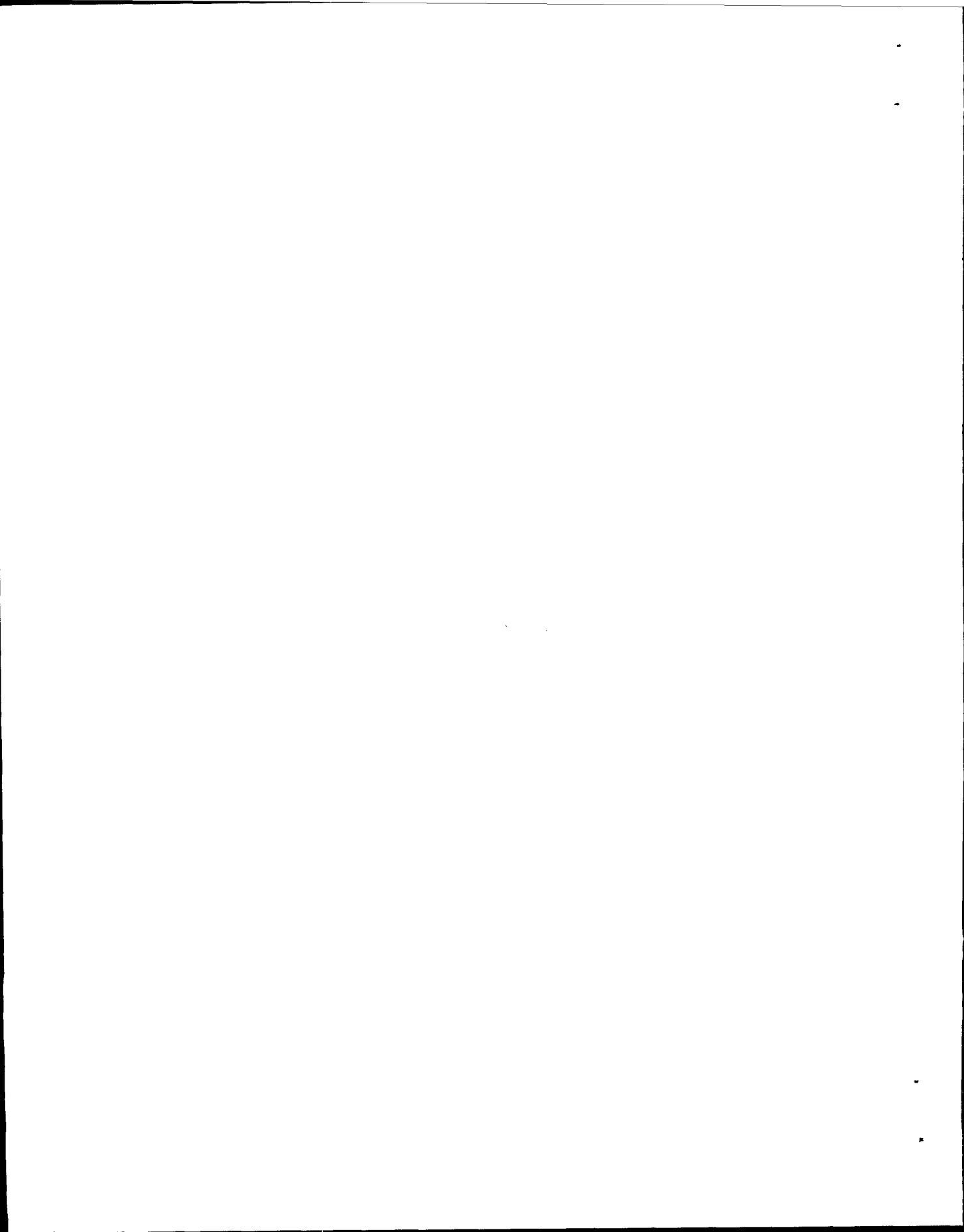
Each integer unit in the numbers represents a depth of 0.005 in., although a zero reading on the gage does not correspond to zero water depth. To obtain the reading corresponding to a zero depth, a gage block with a known height of 0.5 in. (shown in each figure) was used. Thus, the zero depth reading can be obtained and, since each integer unit represents a water depth of 0.005 in., the actual water depths can be found.

The use of this type of data to predict wake Froude number profiles and the results of these predictions are presented in Volume I.

These contour maps are obtained in full-scale although they are reduced in Figures 15, 16, and 17 for report purposes. Hence, this method also provides an accurate way of obtaining any type of data that can be obtained with the sequence-still technique. The stereo method, however, is comparatively less economical and quick and requires special reduction equipment.

SECTION VI - CONCLUSIONS

The tow channel is a useful instrument in the qualitative study of two-dimensional gas flow patterns and trends and, under some conditions, can be used to predict quantitatively two-dimensional gas results. Still photographic techniques are particularly suitable for obtaining data trends in water resulting from changes in independent parameters such as free-stream Froude number (analogous to Mach number in a gas) and body geometry. These techniques provide a means of obtaining such information in a comparatively fast and economical manner. The stereo photographic technique is more time-consuming than still methods and requires special reduction equipment. In addition to providing a means of obtaining the same type data, however, it can also be used to obtain water depth values in the free-stream, inviscid flow, and wake regions. Consequently, the stereo method can be applied to the quantitative study of compressible gas flows.



APPENDIX A - PRINCIPLES OF THE GAS-HYDRAULIC ANALOGY

1. THEORY

The following is a condensation of the derivation of the gas-hydraulic analogy as given by Preiswerk¹ and others.²⁻⁵

Consider the flow of an incompressible fluid through an elementary volume of variable height (see Figure 18). If there is no flow variation in the vertical direction, the equation of continuity gives

$$ud \, dy + vd \, dx = \left(u + \frac{\partial u}{\partial x} dx \right) \left(d + \frac{\partial d}{\partial x} dx \right) dy + \left(v + \frac{\partial v}{\partial y} dy \right) \left(d + \frac{\partial d}{\partial y} dy \right) dx.$$

This equation reduces to

$$\frac{\partial(ud)}{\partial x} + \frac{\partial(vd)}{\partial y} = 0. \quad (9)$$

For a two-dimensional compressible gas flow, the equation of continuity gives

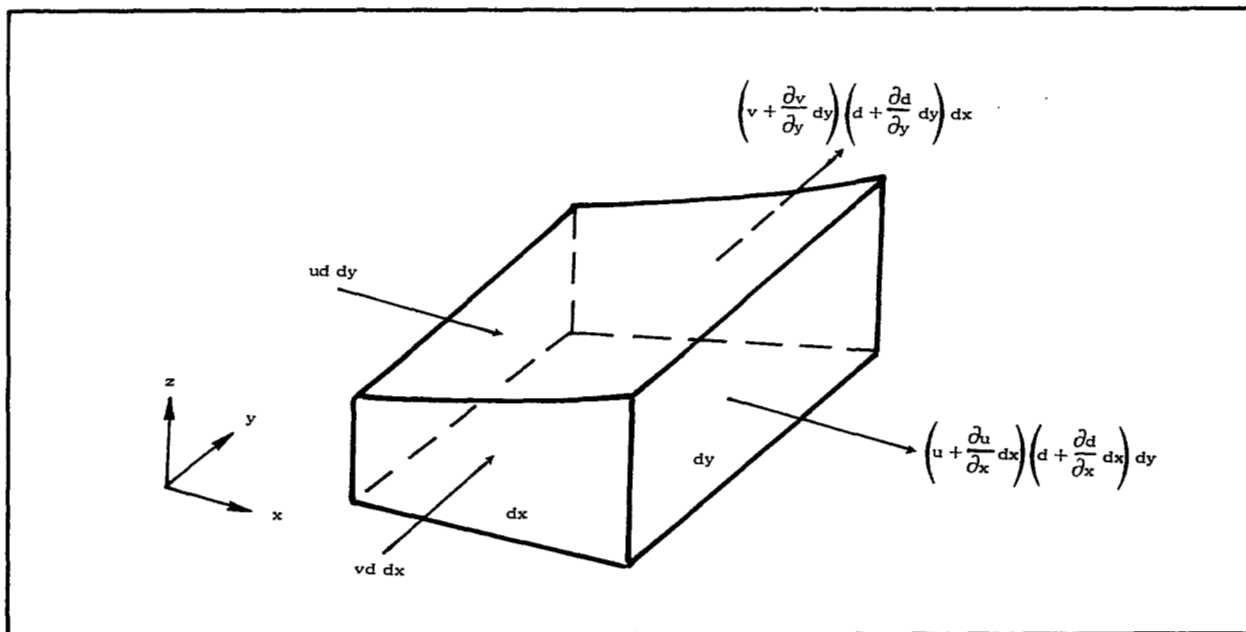


Figure 18 - Flow of Incompressible Fluid

$$\rho u dy + \rho v dx = \left(\rho u + \frac{\partial(\rho u)}{\partial x} dx \right) dy + \left(\rho v + \frac{\partial(\rho v)}{\partial y} dy \right) dx.$$

This equation reduces to

$$\frac{\partial(\rho u)}{\partial x} + \frac{\partial(\rho v)}{\partial y} = 0. \quad (10)$$

Comparing Equations (9) and (10), it is apparent that the water depth and gas density are completely analogous. Hence, expressed nondimensionally as the ratio of static-to-stagnation conditions, the following results are obtained:

$$\frac{\rho}{\rho_0} = \frac{d}{d_0}. \quad (11)$$

In the energy equation, at any point in the fluid flow the sum of the potential and kinetic energy must equal the sum at any other point. For incompressible water flow, where it is assumed that vertical accelerations are negligible compared with gravity, the velocity is given by

$$V^2 = 2g(d_0 - d) \quad (12)$$

and

$$V_{\max}^2 = 2gd_0.$$

Thus, the velocity ratio is given by

$$\left(\frac{V}{V_{\max}} \right)^2 = \frac{d_0 - d}{d_0},$$

or

$$\frac{d}{d_0} = 1 - \left(\frac{V}{V_{\max}} \right)^2 \quad (13)$$

for water.

For a perfect gas, the energy equation reduces to

$$V^2 = 2gc_p(T_0 - T)$$

Therefore,

$$V_{\max}^2 = 2gc_p T_0, \quad (14)$$

where

$$h = gc_p T, \quad (\text{gas enthalpy}).$$

The velocity ratio then is given by

$$\left(\frac{V}{V_{\max}}\right)^2 = \frac{T_o - T}{T_o},$$

or

$$\frac{T}{T_o} = 1 - \left(\frac{V}{V_{\max}}\right)^2 \quad (15)$$

for a gas.

Comparing Equations (13) and (15), it is apparent that the water depth ratio is equivalent to the gas temperature ratio - that is,

$$\frac{d}{d_o} = \frac{T}{T_o} \quad (16)$$

For an isentropic flow, the static-to-stagnation density ratio can be expressed as a function of the static-to-stagnation temperature ratio - that is,

$$\frac{\rho}{\rho_o} = \left(\frac{T}{T_o}\right)^{\frac{1}{\gamma - 1}} \quad (17)$$

Substituting water depth ratios for the analogous depth and temperature ratios gives

$$\frac{d}{d_o} = \left(\frac{d}{d_o}\right)^{\frac{1}{\gamma - 1}} \quad (18)$$

The only value of γ for which this equation holds is $\gamma = 2$. Thus, a flow of water is analogous to a gas only when $\gamma = 2$.

For an isentropic gas flow, the static-to-total pressure ratio can be expressed as a function of the static-to-total density ratio by

$$\frac{p}{p_o} = \left(\frac{\rho}{\rho_o}\right)^\gamma \quad (19)$$

Since it was shown that γ must equal 2, it follows from Equation (18)

$$\frac{p}{p_0} = \left(\frac{\rho}{\rho_0} \right)^2 = \left(\frac{d}{d_0} \right)^2 . \quad (20)$$

Thus, for the conditions specified, it has now been shown that the water depth is analogous to the density, square root of the pressure, and the temperature of a two-dimensional compressible gas.

For an irrotational flow, the differential form of the potential function for a water flow having a free surface can be derived. This equation then can be compared with the corresponding gas equation to show that a water velocity value of \sqrt{gd} is analogous to the sonic velocity, a , in a compressible gas. This is accomplished as follows:

Equation (12) can be rewritten as

$$d = d_0 - \frac{V^2}{2g} = d_0 - \frac{u^2 + v^2}{2g} . \quad (21)$$

Taking the partial derivatives with respect to x and y , there results

$$\frac{\partial d}{\partial x} = -\frac{1}{g} \left(u \frac{\partial u}{\partial x} + v \frac{\partial v}{\partial x} \right)$$

and

$$\frac{\partial d}{\partial y} = -\frac{1}{g} \left(u \frac{\partial u}{\partial y} + v \frac{\partial v}{\partial y} \right) . \quad (22)$$

Substituting these two relationships into the expanded form of Equation (9) gives

$$\frac{\partial u}{\partial x} \left(1 - \frac{u^2}{gd} \right) - \frac{uv}{gd} \left(\frac{\partial u}{\partial y} + \frac{\partial v}{\partial x} \right) + \frac{\partial v}{\partial y} \left(1 - \frac{v^2}{gd} \right) = 0 . \quad (23)$$

For an irrotational flow,

$$\frac{\partial v}{\partial x} - \frac{\partial u}{\partial y} = 0 . \quad (24)$$

Therefore a potential function, ϕ , can be defined so that

$$\frac{\partial \phi}{\partial x} = u ,$$

and

$$\frac{\partial \phi}{\partial y} = v . \quad (25)$$

Substituting these values into Equation (23) gives

$$\phi_{xx} \left(1 - \frac{\phi_x^2}{gd} \right) - 2\phi_{xy} \frac{\phi_x \phi_y}{gd} + \phi_{yy} \left(1 - \frac{\phi_y^2}{gd} \right) = 0. \quad (26)$$

The corresponding gas relationship is (from Reference 2)

$$\phi_{xx} \left(1 - \frac{\phi_x^2}{a^2} \right) - 2\phi_{xy} \frac{\phi_x \phi_y}{a^2} + \phi_{yy} \left(1 - \frac{\phi_y^2}{a^2} \right) = 0. \quad (27)$$

Comparison of Equations (26) and (27) shows that they are identical when

$$a^2 = gd. \quad (28)$$

For shallow water, it can be shown (see Item 2 below) that the surface wave propagation velocity, c , in water is given to a good approximation by

$$c = \sqrt{gd}. \quad (29)$$

The ratio of the local velocity in water to the surface wave propagation velocity defines the Froude number - that is

$$Fr = \frac{V}{c} = \frac{V}{\sqrt{gd}}. \quad (30)$$

It can be seen that this parameter corresponds to the Mach number, M , in a compressible gas.

For values of Fr less than one, the water flow is said to be "streaming." If Fr is greater than one, the water is said to be "shooting." In the latter case, under certain conditions, a strong decrease in velocity accompanied by a rapid rise in depth may occur within a short distance. An unsteady motion of this type is called a hydraulic jump. Hydraulic jumps are geometrically similar to shock waves in a gas.

2. TOW CHANNEL WATER DEPTH

It is possible to select a water depth for which the surface wave propagation velocity, c , is closely approximated by the velocity value \sqrt{gd} . Because this value corresponds to the sonic velocity in a compressible gas, the proper water depth is of considerable importance. In Reference 3, it is shown that the propagation velocity of a surface wave is actually given by

$$c = \left[\left(\frac{g\lambda}{2\pi} + \frac{2\pi\sigma}{\rho\lambda} \right) \tanh \frac{2\pi d}{\lambda} \right]^{1/2}. \quad (31)$$

where

σ = surface tension

ρ = fluid density

d = water depth

λ = wavelength

For very large values of d , such as might exist in the ocean,

$$\frac{2\pi d}{\lambda} \rightarrow \infty$$

and

$$\tanh \frac{2\pi d}{\lambda} \rightarrow 1.$$

For this condition, then, the value of c becomes

$$c \cong \left(\frac{g\lambda}{2\pi} + \frac{2\pi\sigma}{\lambda\rho} \right)^{1/2} \quad (32)$$

From this equation, it can be seen that the propagation velocity is dependent upon the wavelength, a condition which has no counterpart in a compressible gas.

Where d is small,

$$\tanh \frac{2\pi d}{\lambda} \rightarrow \frac{2\pi d}{\lambda}.$$

Therefore,

$$c \cong \left[\left(\frac{g\lambda}{2\pi} + \frac{2\pi\sigma}{\rho\lambda} \right) \left(\frac{2\pi d}{\lambda} \right) \right]^{1/2},$$

or

$$c \cong \sqrt{gh} \left(1 + \frac{4\pi^2\sigma}{g\rho\lambda^2} \right)^{1/2}. \quad (33)$$

In this case, if $d \rightarrow 0$, then the second term in the parenthetical expression becomes predominant for small λ values.

Qualitatively, then, the water depth, d , is restricted to some range that

is neither too deep nor too close to zero. Crossley and Harleman⁹ have suggested that depths from $1/4$ in. to $1-1/2$ in. are suitable when using a water flow channel. Laitone,³ however, found experimentally that, with water depths greater than approximately $1/4$ in. in a tow channel, the wave propagation velocity began to lose all physical significance, and no given waveform could be propagated without a continuous change in shape. At a water depth of about 0.2 in., Laitone showed that $c \approx \sqrt{gd}$ independent of λ for all $\lambda \geq 1$ in. This also can be shown graphically by plotting Equation (33). Figure 19 shows the results, which indicate that at a depth of about 0.2 in.

$$c \approx \sqrt{gd} = \text{constant}$$

for all $\lambda \geq 1$. Waves corresponding to λ values less than this are capillary ripples, and their effect is almost negligible on the formation of hydraulic jumps.

In a purely theoretical approach, Gupta⁶ later showed the optimum water depth to be 0.19 in.

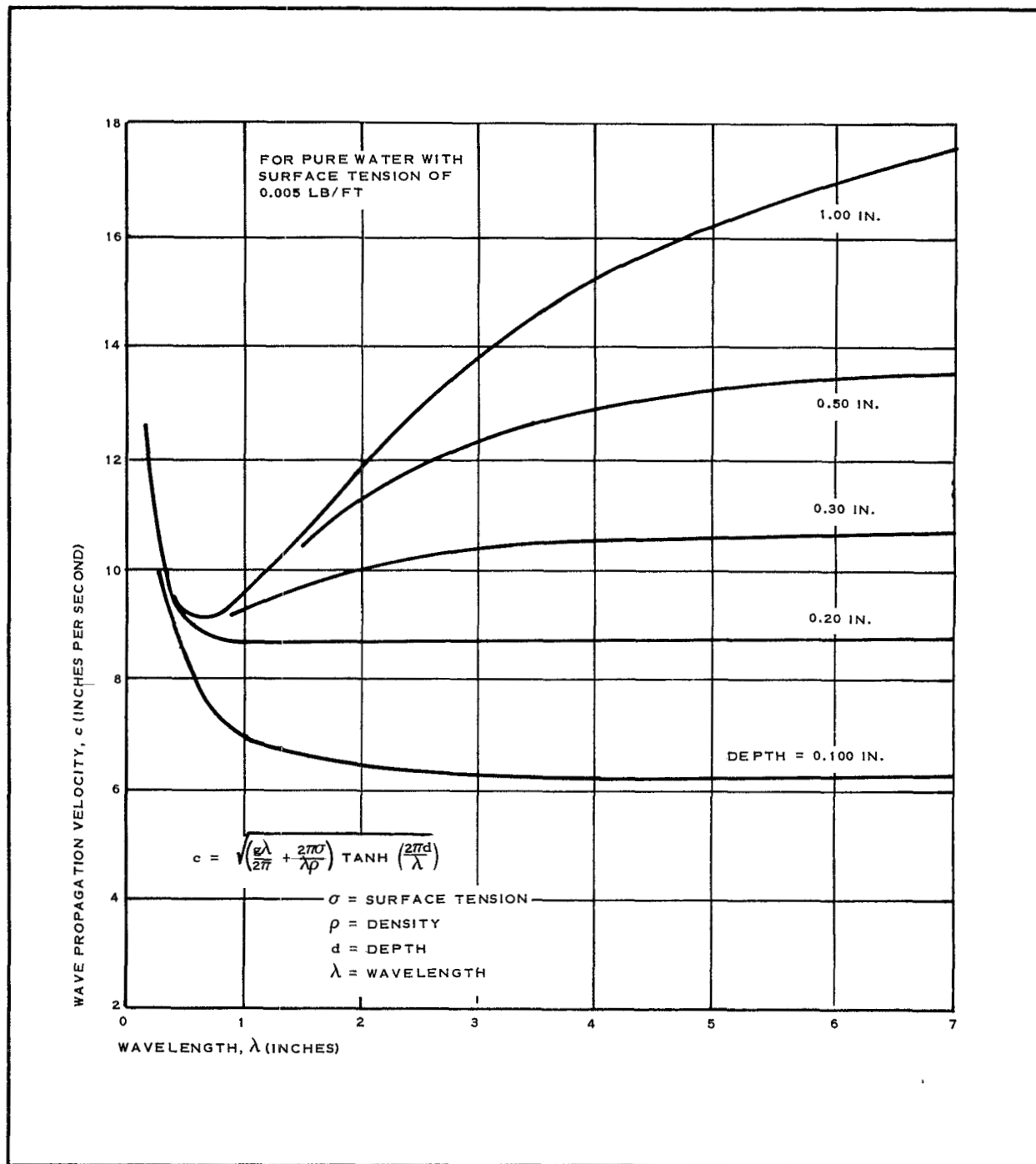


Figure 19 - Surface Wave Propagation Velocity as a Function of Wavelength

APPENDIX B

REPRESENTATIVE TOW CHANNEL STILL PHOTOGRAPHS

Presented in Figures 20 through 39 are typical sequence still photographs obtained during the tow channel test program. Figures 20 through 29 are photographs of single body tests using different representative shapes. Figures 30 and 31 show a 120 deg wedge with a trailing 10 deg wedge (analytical wedge, see Section IV). Finally, Figure 32 through 39 are photographs of either a wedge-block or a 120 deg wedge with a trailing reversed half cylinder (analytical blunt body, see Section IV). In Figures 34, 35, 38, and 39, the forebody is at an angle-of-attack of 5 degrees.

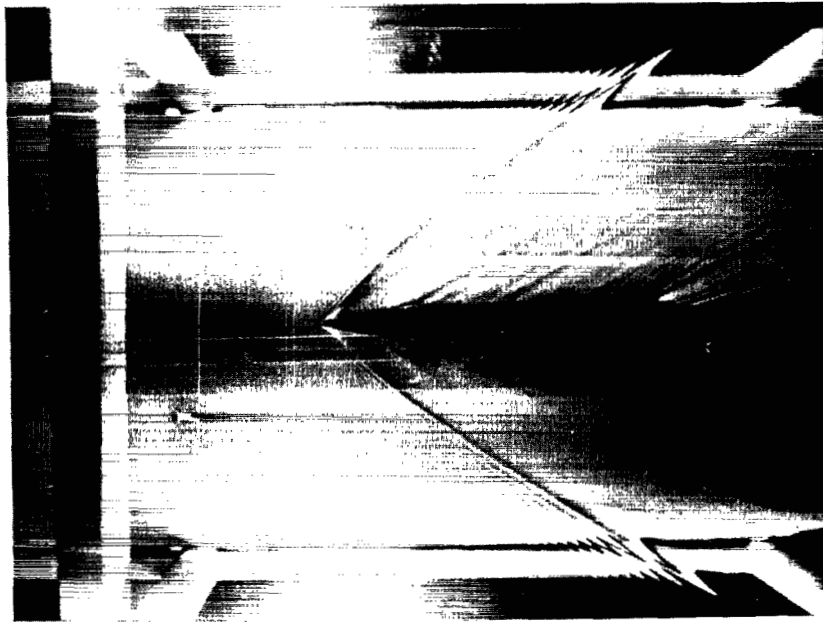


Figure 20 - Wedge-Block ($Fr_{\infty} = 2.0$)

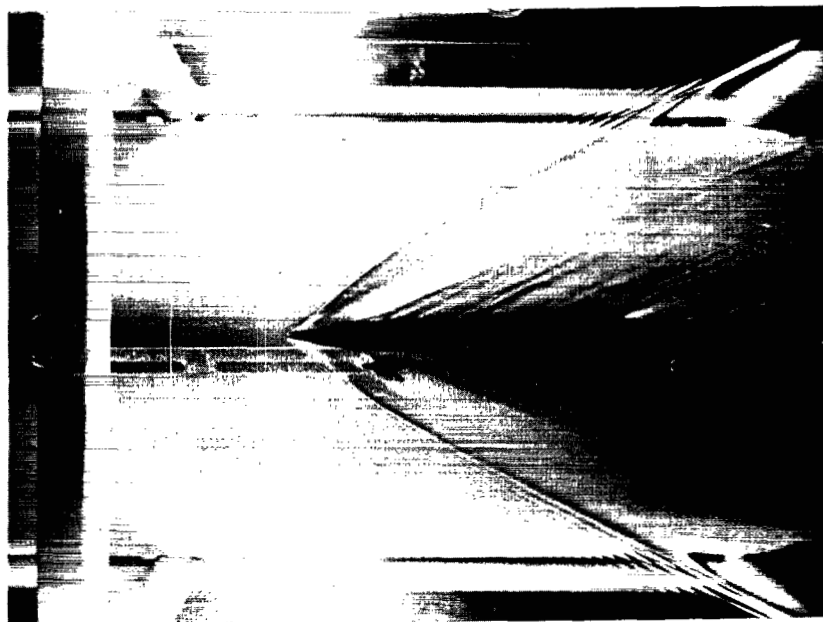


Figure 21 - Wedge-Block ($Fr_{\infty} = 2.5$)

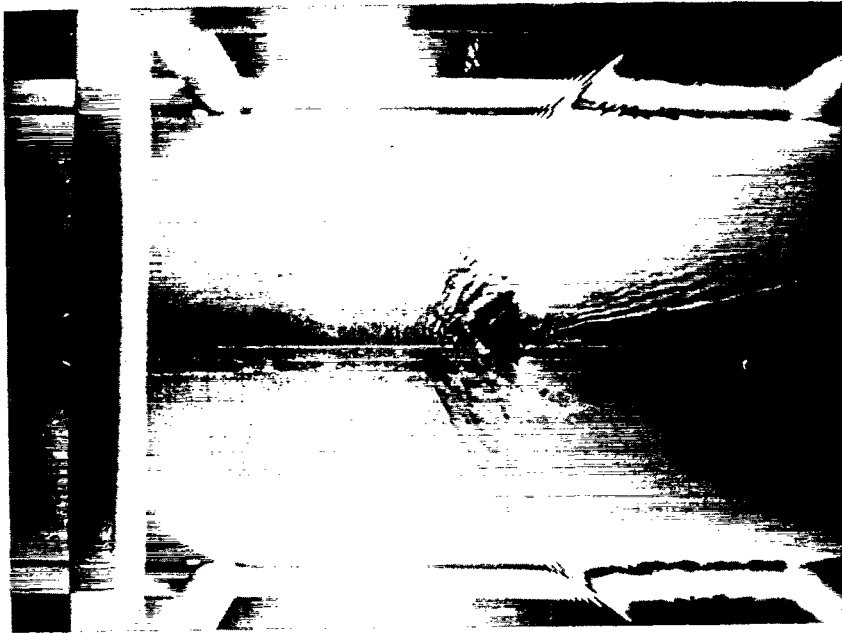


Figure 22 - 80-Deg Wedge ($Fr_{\infty} = 2.0$)



Figure 23 - 80-Deg Wedge ($Fr_{\infty} = 2.5$)

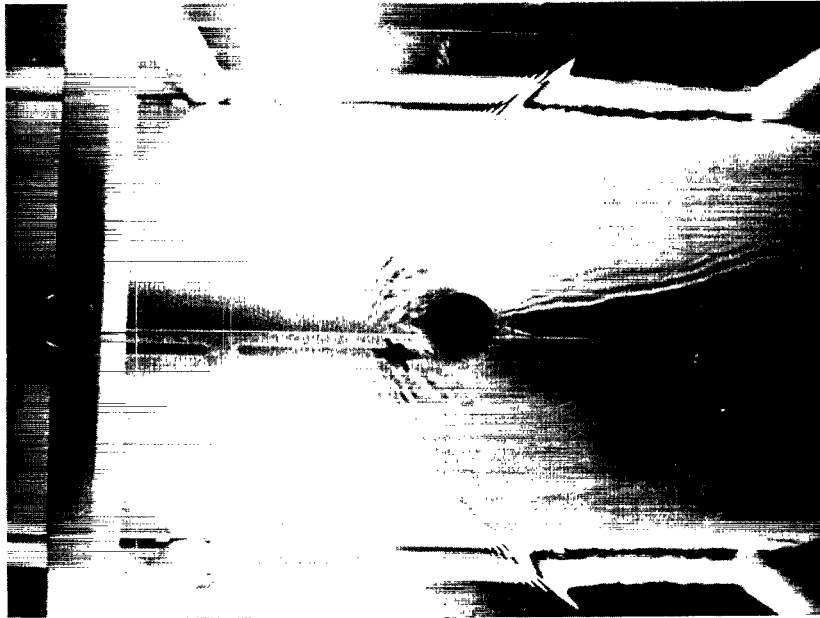


Figure 24 - Circular Cylinder ($Fr_{\infty} = 2.0$)

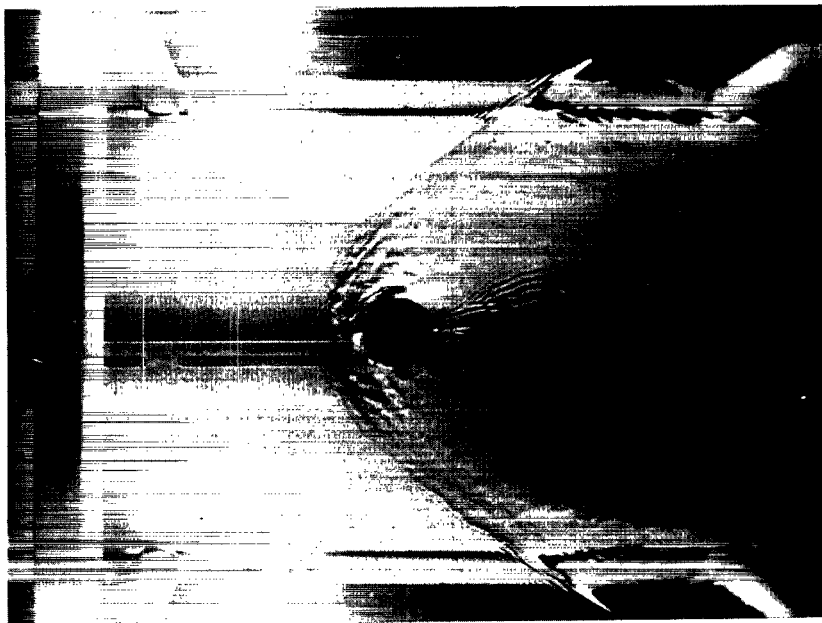


Figure 25 - Circular Cylinder ($Fr_{\infty} = 2.5$)

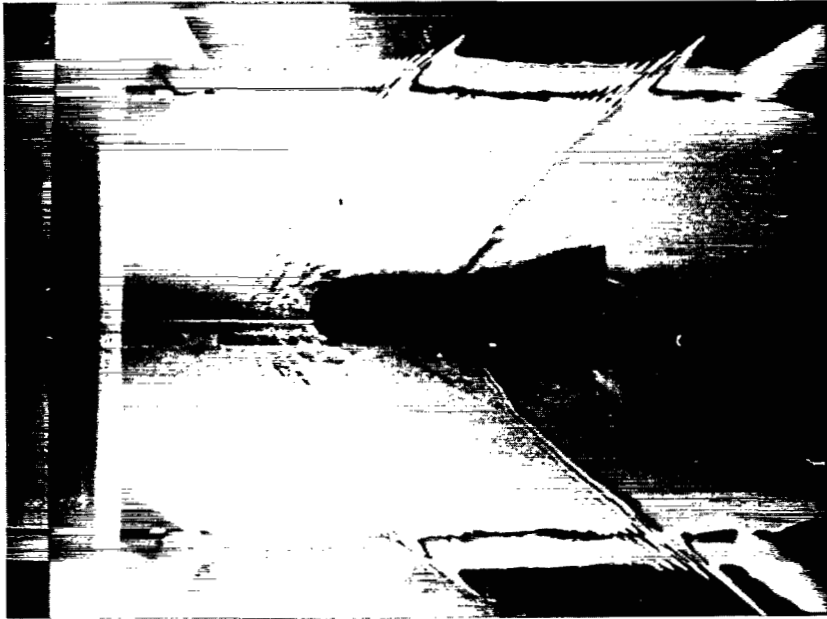


Figure 26 - Half Cylinder-Block-Flare ($Fr_{\infty} = 2.0$)

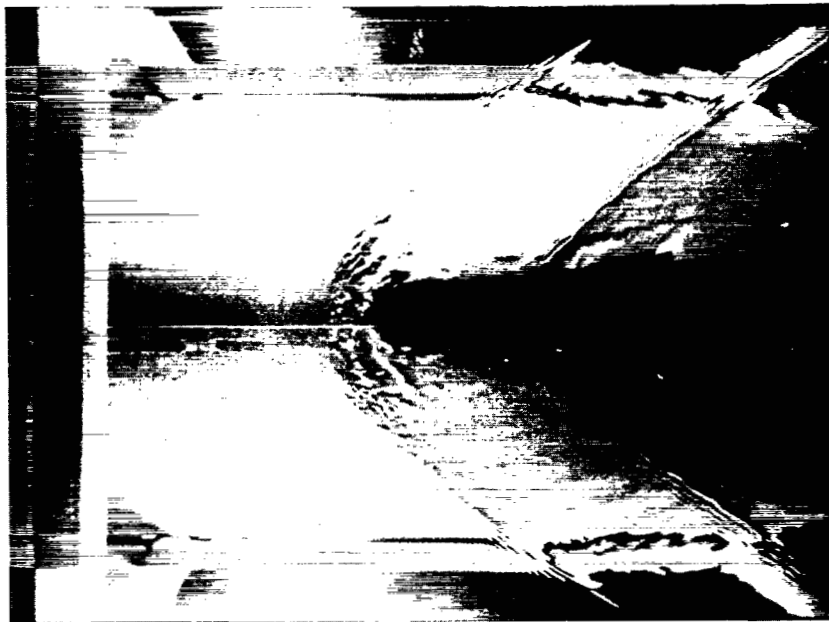


Figure 27 - Half Cylinder-Block-Flare ($Fr_{\infty} = 2.5$)

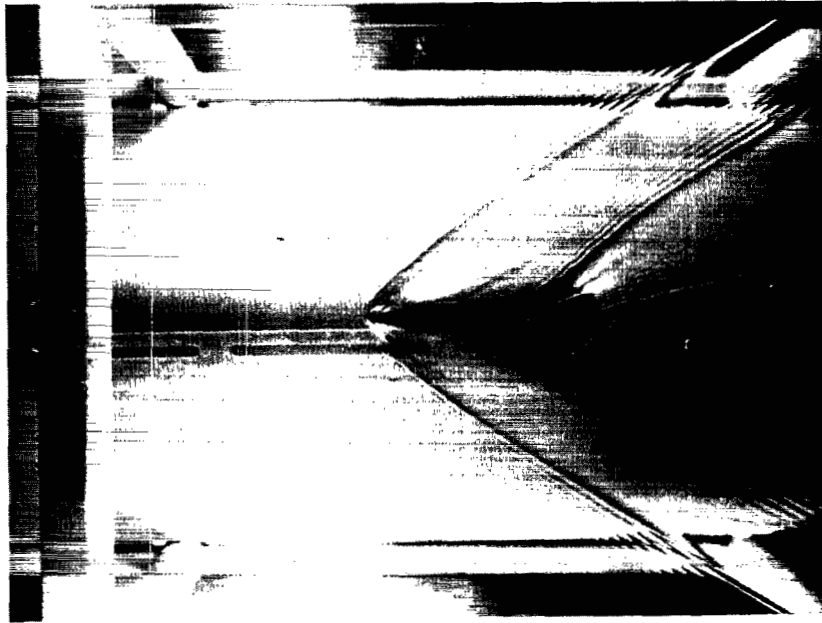


Figure 28 - Blunted Wedge-Block-Flare ($Fr_\infty = 2.0$)

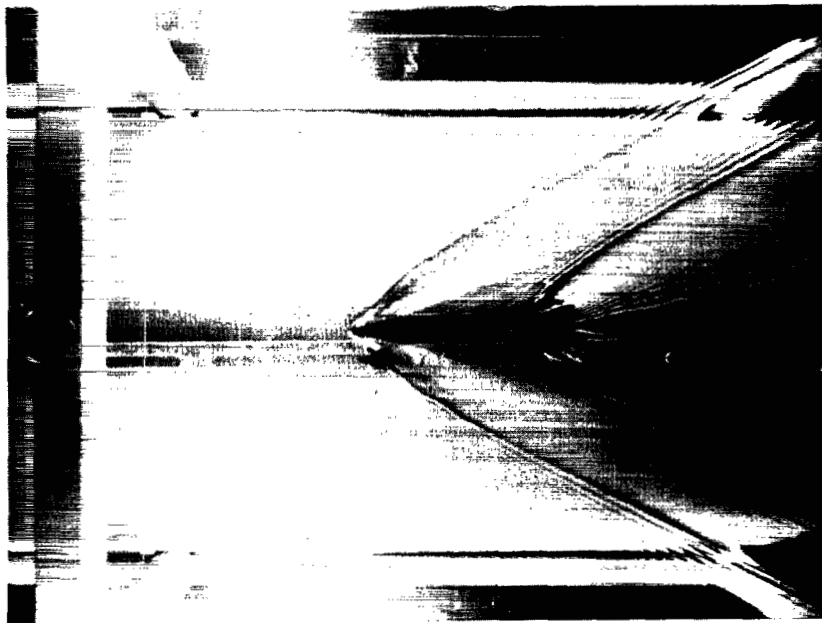


Figure 29 - Blunted Wedge-Block-Flare ($Fr_\infty = 2.5$)



Figure 30 - 120-Deg Wedge with Trailing 10-Deg
Wedge ($Fr_{\infty} = 2.0$, $x/D = 2.0$)

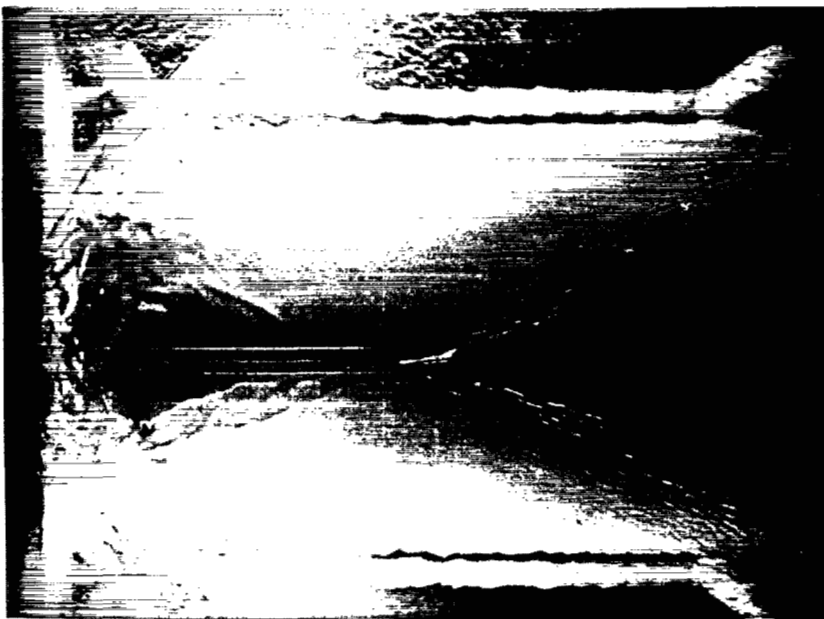


Figure 31 - 120-Deg Wedge with Trailing 10-Deg
Wedge ($Fr_{\infty} = 2.5$, $x/D = 2.0$)

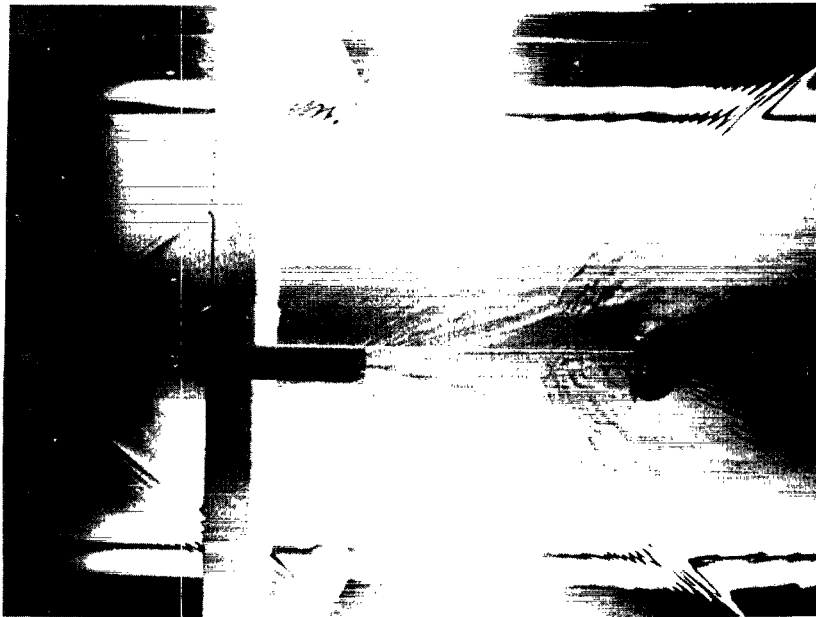


Figure 32 - Wedge-Block with Trailing Reversed
Half Cylinder ($Fr_{\infty} = 2.0$, $x/D = 9$)

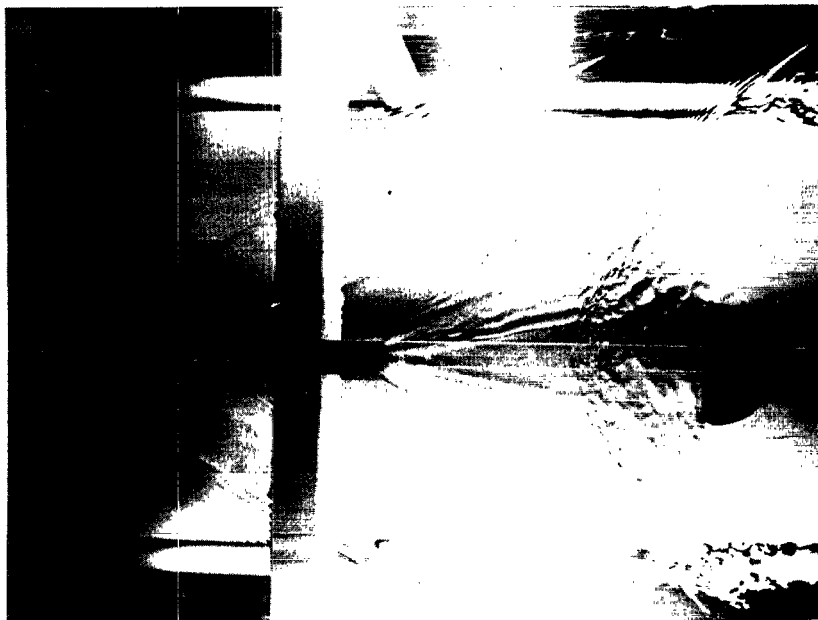


Figure 33 - Wedge-Block with Trailing Reversed
Half Cylinder ($Fr_{\infty} = 2.5$, $x/D = 9$)



Figure 34 - Wedge-Block at $\alpha = 5$ Deg with
Trailing Reversed Half Cylinder
($Fr_{\infty} = 2.0$, $x/D = 9$)

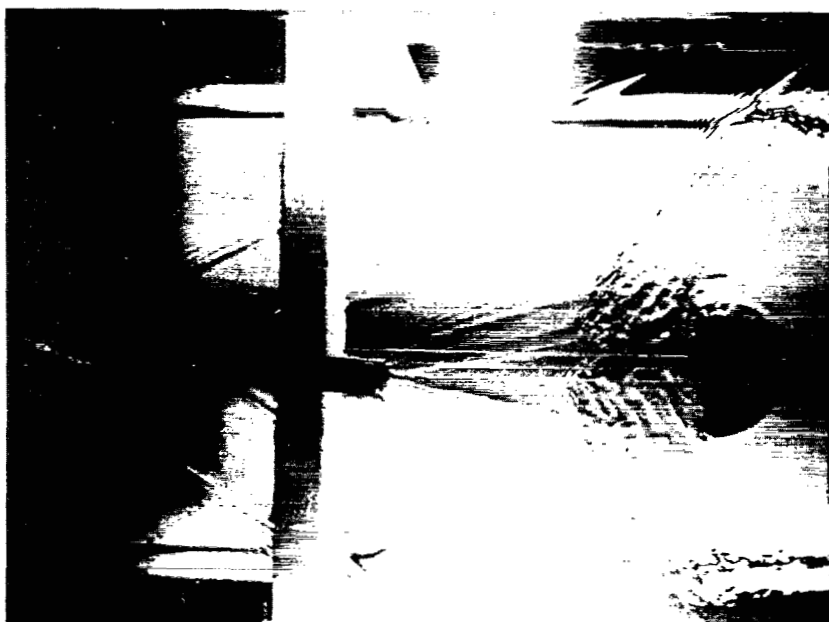


Figure 35 - Wedge-Block at $\alpha = 5$ Deg with
Trailing Reversed Half Cylinder
($Fr_{\infty} = 2.5$, $x/D = 9$)

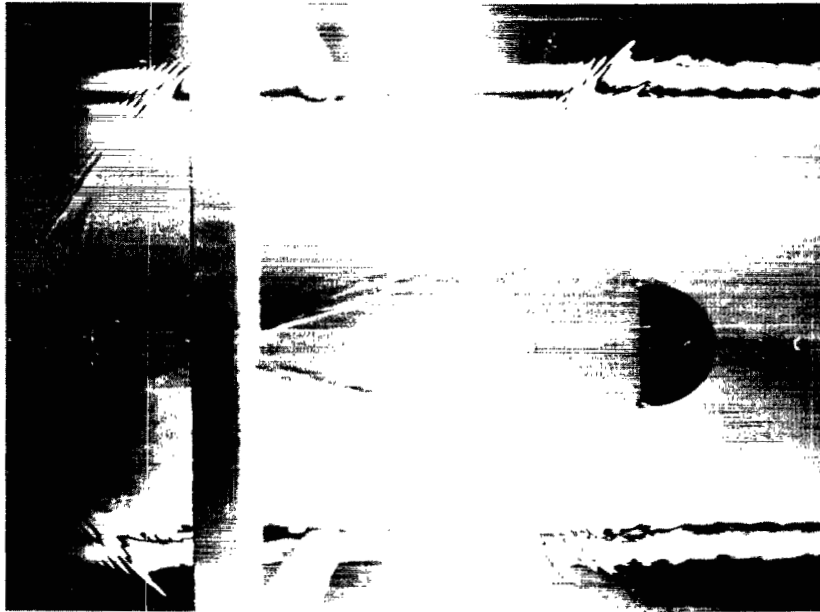


Figure 36 - 120-Deg Wedge with Trailing Reversed Half Cylinder ($Fr_{\infty} = 2.0$, $x/D = 8.5$)



Figure 37 - 120-Deg Wedge with Trailing Reversed Half Cylinder ($Fr_{\infty} = 2.5$, $x/D = 8.5$)

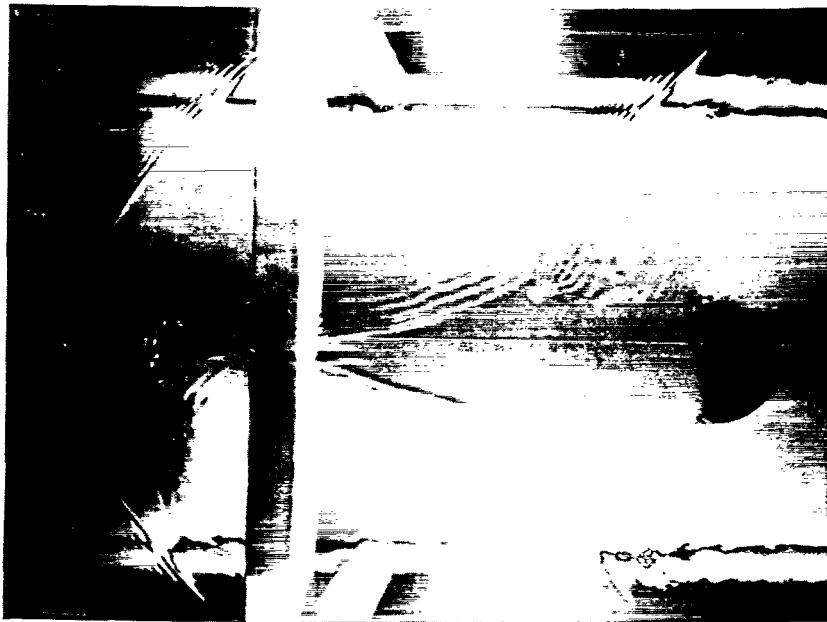


Figure 38 - 120-Deg Wedge at $\alpha = 5$ Deg with
Trailing Reversed Half Cylinder
($Fr_{\infty} = 2.0$, $x/D = 8.5$)



Figure 39 - 120-Deg Wedge at $\alpha = 5$ Deg with
Trailing Reversed Half Cylinder
($Fr_{\infty} = 2.5$, $x/D = 8.5$)

.

.

5

2

LIST OF SYMBOLS

a	sonic velocity
c	surface wave propagation velocity
c_p	heat capacity at constant pressure
D	body diameter, inches
d	water depth, inches
Fr	Froude number
g	gravitational acceleration
h	gas enthalpy
L	body length, inches
l	length
M	Mach number
p	pressure
R	body radius, inches; gas constant
r	radius, inches; transverse coordinate
S	detached bow wave standoff distance, inches
T	temperature
u	axial velocity component
V	velocity
v	lateral or transverse velocity component
x	axial coordinate
x_o	wake neck location measure from forebody base, inches
y	lateral coordinate
α	angle of attack, degrees
γ	specific heat ratio

δ deflection angle
 ϵ trailing wave divergence half angle
 θ bow-wave angle, degrees
 λ wavelength
 ρ density
 σ water surface tension
 ϕ velocity potential function

Subscripts:

b block
f flare
n nose
o stagnation condition
s shoulder
x, y partial differentiation with respect to x or y (e.g., $\phi_x = \partial \phi / \partial x$,
 $\phi_{yy} = \partial^2 \phi / \partial y^2$)
1 reference conditions
2 post wave conditions
 ∞ free-stream conditions

LIST OF REFERENCES

1. Preiswerk, E.: Application of the Methods of Gas Dynamics to Water Flows with Free Surface, Parts I and II. NACA TM 934 and 935, 1940.
2. Orlin, W. J., Lindner, N. J., and Bitterly, J. B.: Application of the Analogy between Water Flow with a Free Surface and Two-Dimensional Compressible Air Flow. NACA Rept. 875, 1946.
3. Laitone, E. U.: A Study of Transonic Gas Dynamics by Hydraulic Analogy. Journal of the Aeronautical Sciences, vol. 19, no. 4, April 1952.
4. Nial, W. R., and Witbeck, N. C.: Water Analogy to Two-Dimensional Air Flow. General Electric (Schenectady) Report No. 55218, August 1941.
5. Heinrich, H. G., and Ibrahim, S. K.: Application of the Water Surface Wave Analogy In Visualizing The Wave Pattern of a Number of Primary and Secondary Body Combinations in Supersonic Flow. WADC Technical Report 59-457, September 1959.
6. Gupta, O. P.: An Analytical Method for Evaluating the Optimum Depth in Hydraulic Analogy Experiments. American Institute of Aeronautics and Astronautics, Vol 3, No. 10, October 1965.
7. Harleman, D. R. F.: Studies on the Validity of the Hydraulic Analogy to Supersonic Flow, Parts I and II. Air Force Technical Report No. 5985, May 1950.
8. Babish, C. H.: Equations, Tables, and Charts for Flow of Shallow Water with a Free Surface. AFFDL-TM-69-2-FDFR, April 1969.
9. Crossley and Harleman, D. R. F.: Studies on the Validity of the Hydraulic Analogy to Supersonic Flow, Part IV. Air Force Technical Report No. 5985, February 1952.